Urban tree architectural modifications over the growing season and water restriction significantly contribute to variations in climate services

Dorine Canonne, Sophie Herpin, Julien Thierry, Camille Bras, Bénédicte Dubuc, Lydie Ledroit, Denis Cesbron, Marc Saudreau, Pierre-Emmanuel Bournet, Sabine Demotes-Mainard

Agricultural and Forest Meteorology 372 (2025) 110694

Contents lists available at ScienceDirect

Agricultural and Forest Meteorology

journal homepage: www.elsevier.com/locate/agrformet

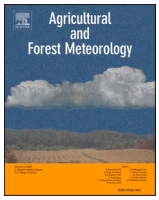

Urban tree architectural modifications over the growing season and water restriction significantly contribute to variations in climate services

Dorine Canonne [a,b,c,d], Sophie Herpin [a,b,c], Julien Thierry [a,b,c,f], Camille Le Bras [c,d], Bénédicte Dubuc [c,d], Lydie Ledroit [c,d], Denis Cesbron [c,d], Marc Saudreau [e], Pierre-Emmanuel Bournet [a,b,c], Sabine Demotes-Mainard [c,d,*]

[a] Institut Agro, UP EPHor, Angers 49000, France
[b] IRSTV, FR CNRS 2488, 3, Nantes 44321 CEDEX, France
[c] QuaSaV, SFR 4207, Angers 49000, France
[d] Institut Agro, Univ Angers, INRAE, IRHS, SFR QUASAV, Angers F-49000, France
[e] Université Clermont Auvergne, INRAE, UMR PIAF, Aubière 63170, France
[f] Ville de Paris, DEVE, STVA, DESV, Paris 75012, France

ARTICLE INFO

Keywords:
Urban environment
Reduced-scale street
Drought
Tree morphology
Shading effect
Transpiration
Human thermal comfort

ABSTRACT

Street trees have gained attention for improving thermal comfort in cities, yet seasonal changes in tree services in relation to the evolution of tree architecture are not well understood. This study hypothesizes that over a growing season and for sunny days, changes in climate services primarily rely on tree architecture influence on cast-shadow, especially during summer droughts. Two alignments of ornamental apple trees were grown in a reduced-scale street canyon, with a non-vegetated control zone. All trees were well watered until July 5th, 2022, after which one alignment experienced moderate water restriction while the other remained well-watered. The street microclimate was characterized, the universal thermal climate index (UTCI) calculated, and tree architecture at the organ and crown scales was measured. On sunny days, well-watered trees improved thermal comfort from 5.8°C UTCI in mid-May to 7.9°C in late August, while water restriction reduced this benefit by up to 2.7°C UTCI after 8 weeks. The changes in thermal comfort were primarily linked to tree architectural development and cast-shadow, although these effects were moderate due to leaf area index high enough in May to ensure 87.5 % of interception of radiation. Increases in crown projected area and volume enhanced tree services, with larger effects on the side than just below the tree canopy. Water restriction diminished thermal comfort by inhibiting stem growth and accelerating leaf fall, thus reducing light interception. This study highlights the significant role of architectural plasticity in tree climate services under water restriction, warranting further research in other species.

Abbreviations

A	individual leaf area (m^2)
a.g.l.	above ground level (m)
AWS	available water storage (%)
C_L	coefficient of leaf area for long axes ($m^2\ m^{-1}$)
C_S	coefficient of leaf area per short axes (m^2)
$\Delta S_{24\ h}$	daily variation of water storage (L)
$\Delta S_{daytime}$	diurnal variation of water storage (L)
Delta(T_a)	air temperature difference between the non-vegetated zone and tree alignments (°C)
$\Delta\Theta_{24\ hours}$	daily variation of the average soil volumetric water content ($cm^3_{water}\ cm^{-3}_{soil}$)
$\Delta\Theta_{daytime}$	diurnal variation of the average soil volumetric water content ($cm^3_{water}\ cm^{-3}_{soil}$)
Delta(T_{mrt})	mean radiant temperature difference between the non-vegetated zone and tree alignments (°C)
Delta(UTCI)	universal thermal climate index difference between the non-vegetated zone and tree alignments (°C)
$ETR_{daytime}$	diurnal evapotranspiration (L $tree^{-2}\ day^{-1}$)
ET_{ref}	reference evapotranspiration (L $m^{-2}\ day^{-1}$)
HTC	human thermal comfort

* Corresponding author at: IRHS, 42 rue Georges Morel, Beaucouzé 49071 CEDEX, France.
E-mail address: sabine.demotes-mainard@inrae.fr (S. Demotes-Mainard).

https://doi.org/10.1016/j.agrformet.2025.110694
Received 25 October 2024; Received in revised form 24 April 2025; Accepted 12 June 2025
Available online 21 June 2025

L	leaf length (m)
LAD	leaf area density ($m^2\ m^{-3}$)
LAI	leaf area index ($m^2\ m^{-2}$)
LVDT	linear variable differential transformer
PAI	plant area index ($m^2\ m^{-2}$)
PEA	projected area of the crown envelope (m^2)
Ψ_{leaf}	leaf water potential measured at midday (Pa)
$\Psi_{predawn}$	Predawn water potential (Pa)
Ψ_{stem}	stem water potential measured at midday (Pa)
r ratio	rate of intercepted short-wavelength radiation by a tree alignment (%)
TLS	terrestrial laser scanner
TLA	total leaf area (m^2)
T_{mrt}	mean radiant temperature (°C)
UTCI	universal thermal climate index (°C)
V_{soil}	soil volume of a tree container (m^3)
VWC	volumetric water content ($cm^3_{water}\ cm^{-3}_{soil}$)
W	leaf width (m)
WR	water-restricted
WW	well-watered

1. Introduction

Ongoing climate changes is marked by an increase in the intensity and frequency of extreme climatic events (IPCC, 2022). In cities, they are enhanced by the urban heat island phenomenon which is characterized by higher air temperature above and within urban areas compared to their rural surroundings, especially during nighttime (Oke, 1973, 1995; Rizwan et al., 2008; Yang et al., 2020; Hartmann et al., 2023). The combination of these two global and micro-climatic concerns is an issue from a public health perspective as city-dwellers consequently experience increased thermal stress (D'Ippoliti et al., 2010; Hanna and Tait, 2015; Arifwidodo and Chandrasiri, 2020). Additionally, the number of people exposed to thermal stress will increase as urban populations grow (United Nations, 2019). Thus, the concept of Human Thermal Comfort (HTC) is increasingly included in public policies with the aim of limiting urban overheating. The HTC can be enhanced by adjusting urban geometry, but finding a trade-off between daytime and nighttime thermal comfort is often challenging. For instance, a lower sky view factor (larger height to width ratio of the street) reduces sun exposure during the day (Jamei et al., 2016), but may trap heat at night (Kleerekoper et al., 2012). Other strategies include watering pavements (Hendel et al., 2014) and utilizing high-albedo materials to reduce heat accumulation (Santamouris et al., 2011). The implementation of urban green infrastructures is also considered a promising approach (Bowler et al., 2010; Lobaccaro and Acero, 2015; Wong et al., 2021). The improvement in HTC provided by urban trees varies depending on parameters such as the site's geometric configuration (Shashua-Bar and Hoffman, 2000) and the type of surface on which they are planted (Kjelgren and Montague, 1998; Konarska et al., 2023; Jiao et al., 2024). Urban trees enhance daytime HTC through cast-shadow and evapotranspiration mechanisms (Nowak and Dwyer, 2007). The cast-shadow provided by urban trees reduces solar radiation reaching the ground beneath the canopy. This prevents heat storage and minimizes long-wave infrared re-emission from mineral areas, leading to reduced surface, air, and mean radiant temperatures (Akbari et al., 2001; Dimoudi and Nikolopoulou, 2003; Lindberg and Grimmond, 2011). As an endothermic reaction, evapotranspiration converts incoming energy into latent heat rather than sensible heat, thereby cooling evaporating surfaces such as tree leaves and their surrounding air (Bowler et al., 2010; Stratópoulos et al., 2018) (Bowler et al., 2010). Nevertheless, urban trees can have adverse effects at night by trapping longwave radiation and reducing ventilation, which may limit cooling and worsen air quality (Morakinyo et al., 2017; Wujeska-Klause and Pfautsch, 2020). Air quality can also be directly affected by tree functioning, as some species emit volatile organic compounds (Khedive et al., 2017).

Several indices can be used to assess HTC (Blazejczyk et al., 2012). Among them, the Universal Thermal Climate Index (UTCI) is particularly relevant as it accounts for all climatic variables, making it universally applicable across a wide range of climates. It is based on the equivalent human physiological responses to combinations of air temperature, radiation, wind and relative humidity (Bröde et al., 2010; Fiala et al., 2012). The UTCI is not very sensitive to relative humidity, except for climates with very warm air temperature combined with high relative humidity (Bröde et al., 2012). The UTCI also shows reduced sensitivity to wind speed in warm conditions encountered during summertime, as the difference between air and skin temperature is then small. Conversely, the UTCI shows a linear relationship with radiation and air temperature (T_a), increasing by 3°C for every 10°C rise in mean radiant temperature (T_{mrt}), and by 1°C for each 1°C increase in T_a. Literature review reported that the T_a reduction between non-shaded and shaded zones provided by urban trees can range from 0.5°C to 8.9°C at pedestrian level depending on assessment methodology (experiment or modeling), the vegetation typology (street trees or treed parks) and density, the street geometry (aspect ratio and orientation) and climate conditions (cold, warm, hot) (Chatzidimitriou et al., 2005; T. Chen et al., 2021; Lai et al., 2019; Loughner et al., 2012; Mballo et al., 2021; Oliveira et al., 2011; Rahman et al., 2018; Richards et al., 2020; Sanusi et al., 2015; Shashua-Bar et al., 2009; Souch and Souch, 1993; Spangenberg et al., 2008; Wang and Zacharias, 2015). Some studies quantified the relative contribution of cast-shadow and evapotranspiration to cooling effect. The cast-shadow by urban trees leads to high T_{mrt} reduction, up to 48.5°C, because tree canopies limit the amount of short-wavelengths radiation reaching the ground, reduce its overheating due to radiative trapping and lower thermal radiative emission (Gillner et al., 2015; Middel and Krayenhoff, 2019; Park et al., 2019). Qiu et al. (2013) reported in their review that the reduction in T_a due to urban vegetation evapotranspiration can range from 0.5°C to 4°C in urban parks, depending on the climate, at 1.8 m to 2.0 m above ground level (a.g.l.). Amounts of energy intercepted by tree canopies and absorbed by evapotranspiration can be assessed from energy considerations but they can vary according to tree characteristics and local conditions. Mballo et al. (2021) quantified the tree shading effect to be responsible for 74 % of tree cooling services, while evapotranspiration only contributed for 26 % from the energetic point of view. These results were obtained from well-watered alignment of ornamental apple trees located in a reduced-scale street canyon with an aspect ratio of 1 in France. In urban space with an aspect ratio $H/W = 0.10$, cast-shadow of well-watered trees located in a similar temperate region in Germany contributed for 55 % when it contributed for 84 % in the hot and arid region of Israel (Shashua-Bar et al., 2009, 2023; Shashua-Bar and Hoffman, 2000).

Both cast-shadow and transpiration are linked to the local climate conditions together with the tree functioning and architectural characteristics. Cast-shadow is linked to the tree architecture that refers to both spatial and dynamic characterization and organization of tree components (Hallé et al., 1978; Godin, 2000; Baïram et al., 2017) and can be formalized by the Beer-Lambert law (Norman and Welles, 1983; Sinoquet et al., 2007). The amount of radiation intercepted can then be related to crown thickness, leaf angle distribution, crown porosity, Leaf Area Index (LAI) or Leaf Area Density (LAD).Tree transpiration is mainly driven by the climatic demand *i.e.* the reference evapotranspiration (ET_{ref}), and is modulated by the tree architecture, its water status and its functional responses (Monteith and Unsworth, 2013).

Urban trees are often subjected to edaphic droughts, which result from water scarcity in urban soils mostly due to high rate of impervious surface in cities and small soil pits (Yu et al., 2018). In summer, edaphic droughts are often combined with atmospheric droughts. The tree functional responses to water availability, encompassing physiological and/or architectural modifications of the tree, depend on species and cultivars. In the short term, tree transpiration is reduced if stomata close as an acclimatization to water deficit (Steiner et al., 2014) and the degree of reduction depends on the severity of water restriction and the

drought tolerance strategy of the considered tree species (Scharwies and Dinneny, 2019). A high and fast falling of the leaves can also occur and lead to a decrease in light interception (Sanusi and Livesley, 2020). In the long term, Devakumar et al. (1999) reported that *Hevea brasiliensis* exposed to dry pre-monsoon conditions had reduced canopy density and branching, leading to lower light interception by summer's end. Effects of drought on urban tree growth were also reported at organ scale by Dale & Frank (2022) who measured lower stem elongations for unwatered *Acer rubrum*, and also by Liu et al. (2022) who reported reduced annual shoot growth in young trees of several species. Cast-shadow can be affected by water restriction in the short, medium and long terms depending on drought intensity and duration, but consequences on climate benefits remained unknown until now. This knowledge-gap is all the more relevant in the context of climate change, where droughts become intense and frequent. Few studies have shown water restriction diminishes climate services provided by urban trees. Moreover, most current studies focus on the climate services reduction through the prism of transpiration effect, neglecting the potential effects of the tree architectural modifications due to water scarcity. Yet, urban trees in water scarcity conditions rely more on their shading effect rather than transpiration to cool the surrounding area (Shashua-Bar et al., 2023; Thierry et al., 2024).

The involvement of below canopy physical variables such as radiation, wind and temperature in thermal comfort (Bröde et al., 2010) implies that the climatic services provided by trees should evolve throughout the growing season, as the canopy develops or according to its phenology (Su et al., 2020). Massetti et al. (2019) reported a decrease in Plant Area Index (PAI) from 5.4 to 2.5 m^2 m^{-2} from early September to mid-November. This decrease was correlated with an increase in the short-wavelength radiation transmitted by the tree canopy from 40 W m^{-2} to 200 W m^{-2}, leading to a reduction in tree shading. Georgi & Zafiriadis (2006) found that the rate of T_a reduction measured under park tree canopies was an exponential function of the radiation transmitted by the canopies. Lindén et al. (2016) have investigated variability of tree transpiration depending on time of day and weather conditions. Meili et al. (2021) used a modeling approach and showed that tree climate services are influenced by seasonal changes, and concluded that seasonal changes do not affect similarly tree climate services depending on the considered region climate. Climate services vary more under temperate climate with higher levels during warm season, whereas in tropical climates, seasonal variations of tree climate services are less pronounced. Even if conceptual links between tree architecture modifications and consequences on below canopy microclimate are obvious, the quantification of the variations in climate services is still needed. Also, the extent to which these variations are linked to tree architectural or physiological modifications remains unclear.

Our objective is to quantify and explain the evolution of climatic services provided by an alignment of trees of the same species in a street canyon over the warm part of a growing season, under well-watered and water-restricted conditions. This work addresses two knowledge gaps: the effects of water restrictions on the climate benefits provided by trees, particularly concerning shading services, and the impact of seasonal architectural changes, influenced by water conditions, on these climate benefits. We hypothesize that during a growing season and for sunny days, (i) tree architectural changes lead to variations in tree climate services and that this is mainly due to changes in shading rather than changes in transpiration; and (ii) that this hypothesis is valid both when trees are well-watered or under water restriction. In this prospect, two alignments of ornamental apple trees were grown in a reduced-scale street canyon facility which included a non-vegetated zone. The tree alignments were subjected to contrasting water regimes. Utilizing a reduced-scale facility allowed for accurate ecophysiological characterizations and bioclimatic measurements at pedestrian height and enabled comparisons of trees with similar histories and conditions, except for the water regime. The results quantify the improvement in HTC provided by trees on sunny days throughout the season and the reduction caused by tree water restrictions. They highlight the primary role of cast-shadow in the variations of climate benefits and identify the tree architectural traits most involved in these changes.

2. Material and methods

2.1. Overall description of the street

The experiment took place in Angers, France (47°28′47″ N, 0°36′33″ W), whose climate is Cfb, meaning mild temperate, without dry season and with warm summer, according to Köppen-Geiger map (Peel et al., 2007). It is also classified as an oceanic climate by the French national meteorological service (Météo-France, 2023). The experiment was run inside a 1/5th reduced scale facility in outdoor conditions, consisting of a street canyon and two meteorological masts. The street is North-South oriented, 15.6 m long and 2 m wide, bordered on each side by a 2 m high building (aspect ratio of 1). The building walls on each side of the street are made of a 0.1 m thick layer of concrete. They are insulated on their inner-side with a 0.12 m thick layer of polystyrene and covered by a white paint on their outer side. The ground of the street is formed by a 0.04 m asphalt layer over a gravel layer.

Such reduced scale street canyon simulates a street measuring 78 m in length, 10 m in width and bordered by 10 m high buildings, at full scale. The use of a reduced-scale street facilitates the study of the tree morphology and ecophysiology, which can be hard in a real urban environment given the size of mature trees. Also, the present model enables the installation of a high density of sensors leading to an accurate and comprehensive characterization of the bioclimatic conditions. The experimental facility was described in detail in Herpin et al. (2024). The question of transposability of results at reduced-scale to full scale have been previously addressed in Mballo et al. (2022) and Herpin et al. (2024).

For the present study, three zones were present inside the street: A Non-Vegetated zone (NV zone) in the southern part of the street, corresponding to the treeless control zone, and two treed zones (with 5 trees each) located in the northern and middle parts of the street, hosting respectively the well-watered (WW) and the water-restricted (WR) tree alignments. The dimensions of each zone and their respective positions are presented in Fig. 1. The trees were grown in containers installed in buried pits, so that their root system was positioned below the ground of the street. To control water inputs and avoid runoff or rainwater from outside, the containers were closed with plastic lids and the pits were covered by cellular polycarbonate plates and asphalt sheets to standardize the radiation properties of the street ground.

2.2. Plant material and growing conditions

Both alignments consisted in ornamental apple trees *Malus Coccinella*® 'Courtarou'. This species was selected as a model species due to its suitability for the dimensions of the experimental setup, allowing for a branched structure with a LAI comparable to urban trees while maintaining a moderate size (Mballo et al., 2021). This species is found in urban environments, although ornamental apple trees are usually planted individually rather than in alignment. Additionally, there is knowledge available about apple tree architecture and ecophysiology. The 10 trees of the experiment were grown from cuttings in nursery and installed in the street on January 19, 2022, aged just over 3.5 years at that time. Each alignment consisted of a northern and a southern border tree, between which were placed the 3 central trees of each alignment that were studied. The flowers were removed manually to prevent the appearance of fruits. A structural pruning was carried out in winter, on February 4, 2022. In order to respect the reduced scale of the street canyon, a trimming was operated on the 10 trees on June 23, 2022, and consisted in cutting back the tree crowns to 1.55 m from the street ground and 0.40 m from the street walls and also 0.60 m from the trunk at the North and South end of each alignment. Trees were irrigated daily

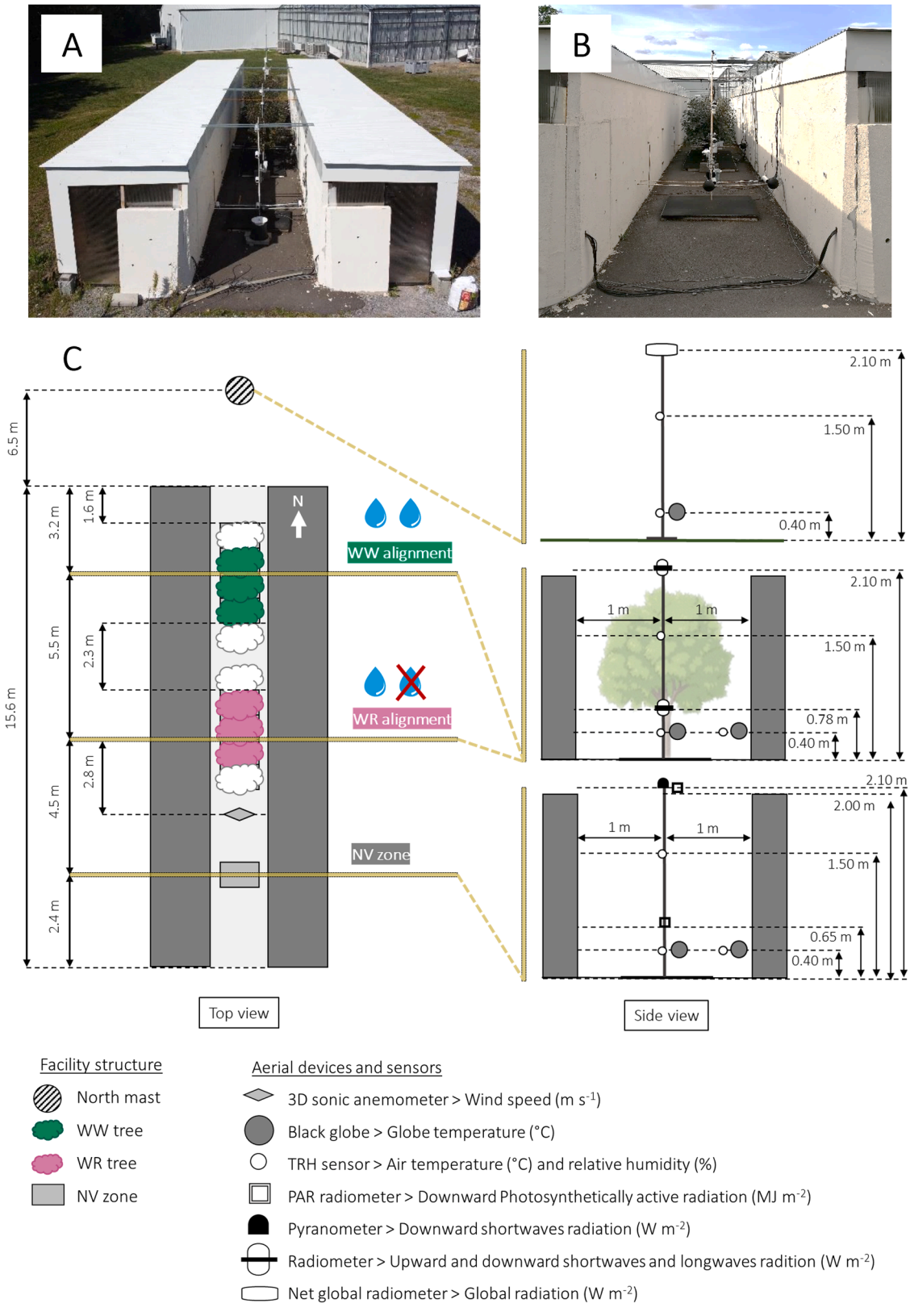

Fig. 1. (. A) Top view picture, (B) front view picture (South of the street) and (C) structure of the facility, composed of a meteorological mast and a street canyon divided in three instrumented zones.

with fertilized water (Plant-Prod 15–10–30; electrical conductivity 1.35 mS/cm; pH 7.5). The only source of water for trees was provided by an irrigation conducted with four drippers per tree.

2.3. Soil conditions and measurement of soil volumetric water content

Each tree was planted inside an 80 L container filled with a 46.3 L mixture of 60 % topsoil / 40 % compost in volume ratio, hereafter

named *soil* (see Thierry et al. (2024) for details). Such a ratio of topsoil/compost is commonly used in urban greening and facilitates the air and water spreading (Cannavo et al., 2014). Below this soil, and separated by a geotextile, a layer of stones and a concrete slope ensured drainage. To measure the soil volumetric water content (VWC), two capacitive probes (EC-5, Decagon Devices Inc., Pullman, USA) were installed in the soil of the three central trees of each alignment, at a depth of about 17 cm over a total of 33 cm, to the north and south side of the container. Soil VWC measurements were used as indicators of the soil water status, based on three thresholds values: the field capacity, the permanent wilting point and the limit between readily Available Water Storage (AWS) and non-readily AWS. These thresholds were expressed in VWC and corresponded respectively to the maximum VWC the soil can retain after gravitational drainage, the minimum VWC accessible to trees, and the point separating water that is easily accessible to plants from water that becomes limiting to plant function.

The field capacity was estimated at 0.28 cm^3_{water} cm^{-3}_{soil} (28 %), based on an experimental water retention curve of the soil used in this experiment, established in the laboratory (French standard NF EN 13,041). The permanent wilting point depends on the soil texture but also on plants. Thus, this threshold was defined using *in-situ* data from probes as 0.10 cm^3_{water} cm^{-3}_{soil} (10 %), since soil VWC did not decrease below this limit. The total available water storage was then 18 % and the limit between readily AWS and non-readily AWS was set to 19 %, corresponding to half of the total available water storage, as indicated for apple trees (Allen et al., 1998).

2.4. Water management

The trees of the WW alignment were well-watered over the whole experimental period. For these trees, the same water dose was delivered daily between 20:00 UTC and 22:00 UTC by drippers. This water dose evolved along time according to the climatic demand and the crown development. The well-watered conditions were obtained by checking the presence of water drainage in the morning after irrigation and monitoring the soil VWC from the values of the capacitive probes, so that they were above 19 % to remain within the readily AWS. The so-called WR alignment were well-watered during the 1st phase of the experiment till July 4, 2022, and then experienced water restriction during the 2nd phase of the experiment from July 5, 2022, to September 14, 2022. Consequently, the trees of the WR alignment were not irrigated on July 5 and 6. Since the trees were irrigated in late evening, water availability differed between modalities during the day from July 6, 2022 onwards. Then, WR trees were irrigated with a reduced water dose first for the next five days until July 11 and then every two days until July 19, to make their soil VWC drastically decrease. From July 19 until September 14, WR trees were irrigated every day with a similar small water quantity, which was adjusted according to the climatic demand. Throughout the entire experimental period, irrigation dose varied from 2.4 L $tree^{-1}$ day^{-1} to 7.2 L $tree^{-1}$ day^{-1} to ensure well-watered conditions, while it ranged from 0.24 L $tree^{-1}$ day^{-1} to 0.56 L $tree^{-1}$ day^{-1} for trees under water restriction.

2.5. Tree transpiration and reference evapotranspiration

Tree transpiration was evaluated using a simplified daily water balance. As transpiration was assumed to occur mainly during daytime, when no irrigation and drainage took place, it was calculated from 05:30 UTC to 19:30 UTC as in Mballo et al. (2021):

$$ETR_{daytime} = -\Delta S_{daytime} = -\Delta\Theta_{daytime}\, V_{soil} \quad (1)$$

with $ETR_{daytime}$ the diurnal evapotranspiration (L), $\Delta S_{daytime}$ the diurnal variation of water storage (L), $\Delta\Theta_{daytime}$ the diurnal variation of the average soil volumetric water content (cm^3_{water} cm^{-3}_{soil}) and V_{soil} the soil volume in each container (L).

This simplified water balance was suitable to estimate transpiration of well-watered trees, because enough water was provided to obtain reliable data from the capacitive probes. Conversely, during water restriction the distribution of water in the soil may be heterogeneous and $\Delta\Theta$ was small compared to irrigation. The transpiration of water-restricted trees was then adapted to take account of the irrigation (Thierry et al., 2024):

$$ETR_{daytime} = I - \Delta S_{24\ hours} = I - \Delta\Theta_{24\ hours}\, V_{soil} \quad (2)$$

with $ETR_{daytime}$ the diurnal evapotranspiration (L), I the irrigation (L), $\Delta S_{24\ h}$ the daily variation of water storage (L), $\Delta\Theta_{24\ h}$ the daily variation of the average soil volumetric water content (cm^3_{water} cm^{-3}_{soil}) and V_{soil} the soil volume of a tree container (L).

The daily climatic conditions were characterized by considering the daily reference evapotranspiration ET_{ref} calculated using the Penman-Monteith equation (Allen et al., 1998) and expressed in L m^{-2} day^{-1}. ET_{ref} provides information on the climatic demand. It was calculated using microclimate sensors at 2 m height on the North and West Mast outside the street (see Section 2.8 for the sensor description).

2.6. Indicators of tree water status: tree water potential measurements and trunk diameter variations

Tree predawn water potential ($\Psi_{predawn}$), tree leaf water potential measured at midday (Ψ_{leaf}) and tree stem water potential measured at midday (Ψ_{stem}) were used as indicators of the tree water status (Daudet et al., 2004; De Swaef et al., 2009; Ballester et al., 2014; Dietrich et al., 2018). These three types of water potential were measured with a Scholander pressure chamber (Model 600D, PMS Instrument Company, Albany, USA) on July 5, July 12, July 19, August 9 and August 29, 2022. At each date, for each type of potential, measurements were conducted on 2 to 3 leaves for each of the three central trees of the WW and WR alignments. On the evening prior to predawn water potential measurements, 3 mature, intact leaves were enclosed on the tree in sealed isothermal bags to prevent condensation on the leaf surface. They were sampled at the end of the night, just before sunrise. For solar noon stem water potential measurements, 3 mature, intact leaves per tree were enclosed in light-reflecting, sealed isothermal bags at least 2 h before solar noon to halt transpiration. Their water potential was then assumed to be in equilibrium with that of the supporting stem, and leaves were collected at solar noon. For solar noon leaf water potential measurements, 3 mature, intact, sun-exposed leaves were collected from each tree at solar noon. Each leaf was immediately enclosed in an individual hermetically sealed plastic bag and stored in the dark under cold conditions.

The trunk diameter variations were measured continuously with Linear Variable Differential Transformers (LVDT) (DF/2.5 or DF/5.0, Solartron Metrology, Bognor Regis, United Kingdom) from May 1, 2022, to August 30, 2022. The LVDT were installed on the North face of the trunk of the three central trees of each modality, at 0.62 m height above street ground and trunk diameter variations were recorded every 10 min.

2.7. Tree architectural traits measurements

The evolution over the season of several tree architectural traits were characterized *i)* at the global scale of the crown and *ii)* at the scale of the basic entities constituting the crown (stems and leaves) (Barthélémy and Caraglio, 2007) to investigate the growth and development processes most involved in the evolution of the crown architectural traits according to the period and water availability. Measurements were performed five times from early May to late August 2022, corresponding to a period which includes peaks of hot weather in Angers and when the foliage is expected to undergo noticeable changes. Attention was paid to characterize the architecture before and after trimming, operated on

June 23, 2022. We considered that the architecture did not evolve during the two weeks following trimming, meaning that measurements operated during this period were valid from the day after trimming to 2 weeks later. The methods used to characterize tree architectural traits were adapted to the scale of the studied object, *i.e.* either tree crown, growth unit or leaf. For that reason, 3 different methods were used to get precise metrics from the different studied scales (Table 1).

2.7.1. Lasergrammetry data

Five campaigns of lasergrammetric measurements were carried out over the season (Table 1) to estimate the crown volume, the PEA and the gap fraction of the crown porosity. These data were obtained using a phase-shift Terrestrial Laser Scanner (TLS) (FARO 3D Focus x130, FARO Technologies Inc., Lake Mary, USA). Each tree alignment was referred as the studied scene and 12 stations were identified around it, either at 0.58 m or 1.80 m a.g.l. outside or inside the canopy. On each station and based on a first low-definition acquisition, a high-definition acquisition was performed (color; quality: 3x; resolution: 1/4; (Pimont et al., 2015; Vandendaele et al., 2022)). Both "clear contour" and "clear sky" filters of the device were turned off for all acquisitions. To enable the subsequent consolidation of the acquisitions, 5 target spheres and 4 checkerboards were placed within the scene and remained fixed for the duration of the measurements. The consolidation processing was carried out using the manufacturer's software (FARO SCENE 7.0.0.39, FARO Technologies Inc., Lake Mary, USA). For each measurement date, a 3D point cloud was generated for each tree alignment. A second pre-processing step was performed in CloudCompare (Girardeau-Montaut, 2023) to clean the 3D point cloud by removing all external elements from the scene. From each cleaned 3D point cloud, a concave envelope of the crown alignment was computed using a MatLab script, based on the alphaShape function with a precision parameter *alpha* set to 0.15 (MathWorks, 2013). This enabled volume estimation. Each resulting envelope was then analyzed in CloudCompare to extract the PEA. Finally, all 3D point clouds and their corresponding concave envelopes were processed using the PATH model (Hu et al., 2018) to estimate the gap fraction of the canopy, also referred to as crown porosity. Both volume and PEA were thus obtained at the alignment scale, *i.e.* including the five trees of each alignment.

2.7.2. Manually measured data

Five campaigns of manual measurements were carried out over the season (Table 1) to estimate the number of axes per tree, their average length, their number of leaves, the area of an individual leaf, the rate of defoliation and finally the leaf area per tree. A campaign of manual measurement lasting several days, measurements were alternated between the two treed modalities to avoid introducing temporal bias. Apple trees present a polymorphism of axes with "short" axes that do not have the potential to elongate and count both few leaves and internodes, and "long" axes with more leaves and elongated internodes. Axes longer than 5 cm were classified as *long axes*, and those shorter or equal to 5 cm as *short axes* (Pitchers et al., 2021). Only the axes formed in 2022 and thus bearing leaves were studied and all manual measurements were made on the three central trees of each alignment.

At each campaign, except for the day of trimming, all short and long axes were counted. The length of each long axis was measured with a measuring tape and it was noted whether it had been trimmed or not. Trimming relieved apical dominance and stimulated the axes development from the buds positioned under the cut end. In August 2022, it was thus noted for each axis whether it developed before trimming (axis of generation 1, from now on called G1) or in response to it (axis of generation 2, from now on called G2). When leaves had fallen from a long axis, the length of each contiguous defoliated part was measured (from the middle of the first to the middle of the last internode that had lost a leaf).

For each studied tree and measurement campaign, 10 short axes were randomly selected, while 10 long axes formed prior to trimming (G1 axes) were chosen using stratified random sampling. The stratification was based on positions of the axes within the crown, also corresponding to plagiotropic and orthotropic characteristics (with plagiotropic axes located on the sides and orthotropic axes at the top). Additionally, in August, 10 axes formed after trimming (G2 axes) were sampled using the same procedure as for the G1 long axes. A different set of axes was sampled for each measurement campaign. On each sampled axis the leaves were counted and their length and width were measured with a ruler. The length of the associated axis (for long axes) was measured with a measuring tape. Individual leaf area was then calculated by allometry from the sampled leaves as in (3).

$$A = 0.7149\,LW \tag{3}$$

with A the individual leaf area (cm^2), L the leaf length (cm) and W the leaf width (cm). This equation had been previously established and validated on mature and young leaves of *Malus Coccinella*® 'Courtarou' apple trees. These leaves were scanned and their area, length and width were measured with Fiji software (https://imagej.net/software/fiji/) (for equation establishment: $n = 131$ leaves sampled in 2019, R^2=0.99, $P < 0.001$; for validation: $n = 299$ leaves sampled in June and September 2022, RMSEP=2.73 cm^2, mean bias deviation=−0.19 cm^2).

The average internode length for untrimmed long axes was calculated as the average of the ratio between long axis length to leaf number, separately for G1 and G2 axes. The average number of leaves that had developed per untrimmed long axes was so calculated as the mean length of all long axes of a tree that were not trimmed, divided by the average internode length of untrimmed axes, separately for G1 and G2 axes.

Leaf area per axis was calculated for the sampled axes by summing of the area of all leaves. Subsequently, the coefficient of leaf area for long axes C_L ($m^2\ m^{-1}$) and the coefficient of leaf area per short axes C_S (m^2) were calculated at the sampled-axis scale and then averaged by tree, separately for G1 and G2 axes, as followed:

$$C_L = \frac{LA}{FA} \tag{4}$$

with C_L the coefficient of leaf area for long axes ($m^2\ m^{-1}$), LA the leaf area per axis (m^2) and FA the length of the foliated section of the axis (m).

$$C_S = LA \tag{5}$$

Table 1
Dates of the campaigns of architectural trait measurements, according to the method used. The indicated date refers to the average measurement date for each considered measurement method.

Period of the chosen dates	Lasergrammetry (tree scale)	Manual (growth unit scale)	Digitizing (leaf scale)
In spring, at the beginning of the period when hot days can occur	May 1, 2022	May 1, 2022	May 5, 2022
Few weeks before summer, at a moment when trees were well-developed	June 14, 2022	June 1, 2022	June 16, 2022
The day of trimming	-	June 23, 2022	-
Two weeks after trimming, before the water regimes could impact architecture	July 12, 2022	July 7, 2022	-
Intermediate date in summer during the application of differentiated water regimes	August 11, 2022	-	-
At the end of the period when hot days can occur, after 72 days of differentiated water regimes	September 14, 2022	August 28, 2022	September 6, 2022

with C_s the coefficient of leaf area per short axis (m^2) and LA the leaf area per axis (m^2).

The G2 axes had the ontogenic potential to elongate, as they developed into long axes in the WW alignment trees. However, because they were minimally elongated in the WR tree alignment, the long axes formed after trimming in WR tree alignment were considered as a single axis unit, similar to the short axes. On August 28, 2022, the leaf area borne by G2 axes was estimated using (4) in WW alignment and (5) in WR alignment.

The Total Leaf Area per tree (TLA) was finally calculated in m^2 as followed (6):

$$TLA = \begin{cases} SFA_{G1}\, C_{L,G1} + N_{G1}\, C_{S,G1} + SFA_{G2}\, C_{L,G2} \text{ for WW trees} \\ SFA_{G1}\, C_{L,G1} + N_{G1}\, C_{S,G1} + N_{G2}\, C_{S,G2} \text{ for WR trees} \end{cases} \quad (6)$$

with *TLA* the total leaf area per tree (m^2), SFA_{G1} the sum of the length of foliated sections of all long G1 axes (m), $C_{L,G1}$ the coefficient of leaf area for long G1 axes ($m^2\ m^{-1}$), N_{G1} the number of foliated short G1 axes, $C_{S,G1}$ the coefficient of leaf area per short G1 axis (m^2), SFA_{G2} the sum of the length of the foliated sections of all long G2 axes (m), $C_{L,G2}$ the coefficient of leaf area for long G2 axes ($m^2\ m^{-1}$), N_{G2} the number of foliated short G2 axes, $C_{S,G2}$ the coefficient of leaf area per short G2 axis (m^2).

Since it is considered that architecture undergoes little changes during the two weeks following trimming, measurements taken on July 7, 2022, were considered valid from June 24, 2022, which corresponds to one day after trimming). When trees were trimmed on June 23, 2022, all sections of the axes that were removed by trimming were collected and their lengths were measured. Additionally, the defoliated length was measured for any sections from which leaves had fallen. The length and width of each leaf were measured for one-third of the total number of axes sections removed during trimming. Since only long axes were trimmed, the leaf area suppressed by trimming was calculated for each studied tree using Eqs. (3), (5), (6). The result was added to the leaf area estimated on June 24, 2022, to calculate the leaf area per tree on June 22, 2022, just before trimming.

Defoliation rate on G1 long axes was calculated at tree level as the cumulative length of all defoliated lengths of G1 long axes divided by the cumulative length of all G1 long axes. The same calculation was applied to G2 axes to estimate the defoliation rate on G2 axes.

2.7.3. Combined data from lasergrammety and manual measurements

The Leaf Area Index (LAI, $m^2\ m^{-2}$) and the Leaf Area Density (LAD, $m^2\ m^{-3}$) were estimated at the alignment scale using a combination of lasergrammetry and manually collected data. They were calculated as the ratio between the TLA of the tree alignment (m^2) and the projected area of its crown envelope (PEA, m^2) for the LAI, and the volume of its crown alignment (V, m^3) for the LAD (Sinoquet et al., 2007). The TLA for each alignment corresponded to the sum of the leaf area of the five trees forming it. The leaf areas of the three studied trees were measured according to the procedure described in Section 2.7.2, and those of the two bordered trees were estimated as the average of the three known tree leaf areas.

The LAI and LAD were estimated over eight dates, corresponding to the dates of lasergrammetry and manual measurements, except the day of trimming. Since lasergrammetry and manual measurements were not conducted on the same dates, interpolated TLA values were used when PEA or volume data were available and conversely, interpolated PEA or volume values were used when TLA data were available.

2.7.4. Digitizing

The digitizing method was used to estimate the leaf inclination angle, defined as the angle formed between the vertical (pointing upward) and the normal to the leaf midrib (Pisek et al., 2011; Ross, 1981). Thus, an inclination angle of 0° corresponds to a horizontal leaf, +90° and −90° to a vertical leaf pointing upward and downward, respectively. Ten G1 long axes were sampled on each of the three central trees on May 5, June 16 and September 6, 2022 and eight G2 long axes on September 6, 2022. For each leaf, the 3D coordinates of the midrib ends were recorded using a mechanical digitizer (Immersion Microscribe G2L, Solution Technologies, Oella, MD, USA). When the tip of the leaf had a different inclination from the rest of the limb, the most apical point recorded was taken slightly upstream to be representative of the inclination of the majority of the limb. Leaf inclination angle was calculated for each leaf from the 3D coordinates with a R script. The numbers of measured leaves are available in Table 2.

2.8. Meteorological and microclimatic conditions

Meteorological conditions at the experimental site outside the street canyon were recorded both by the Beaucouzé Météo-France station located 400 m from the experimental site, and on the site itself with the North mast placed 6.5 m north from the street. Air temperature and air relative humidity were measured by TRH sensor (HMT330, Vaisala, ±0.2°C on air temperature and ±1.5 % points on relative humidity) on this same mast at 0.40 m, 1.5 m and 2.0 m heights a.g.l. Globe temperature was measured at 0.40 m height using a P100 sensor (RS Pro, $\pm 0.15°C + 0.002 \times T$ (°C)) inside a 15 cm diameter black globe. A net radiometer (NR-Lite2, Kipp&Zonen, accuracy not communicated by manufacturer) at 2.1 m height a.g.l. was installed to characterize incident climatic conditions on the overall experimental facility and to estimate the reference evapotranspiration. A 2D sonic anemometer (CV7, LCJ Capteurs, ±2 % on wind speed and ±3 ° on wind direction) was installed at 2.0 m height a.g.l. on a 2nd meteorological mast (placed at 8.0 m west from the street canyon west building), to provide off-street wind speeds.

Instrumentation was also used inside the street canyon to characterize microclimatic conditions and to study the effect of the tree alignments on the human thermal comfort. To do so, an instrumental vertical plane was installed in the center of each of the three experimental zones. Inside each vertical plane, measurements were mainly realized in the center of the street, to assess the effect of trees at solar noon; some measurements were also realized on the east side of the street (at 0.15 m from the wall) to study the effect of trees in the afternoon, and also to evaluate the change in lateral extent of shading in relation to different tree development in WW and WR modalities. Measurements were mainly realized at 0.40 m a.g.l., corresponding to 2.0 m a.g.l. at full scale, in order to evaluate human thermal comfort (Fig. 1). At 0.40 m a.g.l., air temperature and air relative humidity were measured by TRH sensors (HMP110 and HMT330, Vaisala, ±0.2°C on air temperature and ±1.5 % points on relative humidity) both at the center and on the east side of the street. Globe temperature was recorded at the same positions with a black globe (same sensor and accuracy as in the previous paragraph on the North mast). Wind speed in the center of the street was measured at 0.40 m a.g.l., between WR alignment and NV zone using a 3D sonic anemometer (CSAT-3D, Campbell scientific, ±0.08 m s^{-1} on wind speed and ±0.7 ° on wind direction). At this

Table 2
Number of leaves sampled in the two tree alignments to obtain angular distributions. The median inclination angle at each measurement date for the two tree alignments is reported.

Date	Population of the sampled axes	Studied alignment	Number of measured leaves	Median inclination angle (°)
May 5, 2022	G1	WW	473	−37.2
		WR	417	−28.8
June 16, 2022	G1	WW	593	−28.6
		WR	806	−20.5
September 6, 2022	G1	WW	317	−40.0
		WR	323	−50.1
	G2	WW	675	+4.81
		WR	NA	NA

height, the wind speed was assumed to be almost the same in the three distinct zones of the street, namely the NV zone, the WW tree alignment and the WR tree alignment. In fact, the three zones were quite close to each other and it was reported that wind speed does not impact so much heat stress if air temperature ranges from 30°C to 40°C (Bröde et al., 2012). At 0.78 m and 2.10 m heights a.g.l. in the center of the street, downward and upward long-wavelength and short-wavelength radiations were measured using CNR4 4 component radiometers (CNR4, Kipp&Zonen, ±10 % on daily sums) in WW and WR tree alignments. Short-wavelength radiation was also measured in the NV zone at 2.1 m a.g.l. (CMP3, Kipp&Zonen, ±10 % on daily sums). Additionally, short-wavelength radiation was estimated in the NV zone at 0.65 m a.g.l., by utilizing measurements from PAR radiometers (Li-190SA, Li-Cor, ±1 %) installed at both 0.65 m and 2.0 m a.g.l. The method of estimation is described in detail by Thierry et al. (2024). The associated air temperature, air relative humidity and globe temperature were used to evaluate the spatial extent of the climate services provided by the tree alignments. The data recorded by these sensors were read every 10 s by the data loggers and then averaged over 10 min periods.

2.9. Light interception

The light interception of the trees was calculated as the rate of cumulative short-wavelength radiation intercepted by their crowns (*r ratio*, %). It corresponded to the normalized difference between the downward short-wavelength radiation measured at 0.65 m a.g.l. in the NV zone ($R_{NV,\ 0.65}$, MJ m^{-2}) and downward short-wavelength radiation transmitted by the crowns measured at 0.78 m a.g.l. ($R_{algmt,\ 0.78}$, MJ m^{-2}) in the two tree alignments, cumulated over the solar noon period, *i.e.* from 11:00 UTC to 13:00 UTC (7) (Thierry et al., 2024)(7):

$$r\ ratio = \frac{R_{NV,\ 0.65} - R_{algmt,\ 0.78}}{R_{NV,\ 0.65}} \times 100 \quad (7)$$

2.10. Thermal comfort

The human thermal comfort in the facility was quantified by estimating the UTCI. This index is a bio-meteorological index that provides an estimate of the human physiological response to climate conditions. It assesses the level of thermal stress (Bröde et al., 2010). From an operational point of view, the UTCI corresponds to the air temperature in defined reference conditions,[1] causing the same physiological response as in the studied conditions (Bröde et al., 2012), using a physiological model of the human body (Fiala et al., 2012). The UTCI can be defined as the corrected current air temperature given by Eq. (8).

$$UTCI_{(T_a,T_{mrt},V_a,RH)} = Ta + Offset_{(T_a,T_{mrt},V_a,RH)} \quad (8)$$

with T_a the air temperature (°C), T_{mrt} the mean radiant temperature (°C), V_a the wind speed (m s^{-1}) and RH the relative humidity (%).

The offset expresses the effects of human regulation and clothing, as well as the thermal load induced by variations in the other meteorological variables (wind, humidity and radiation), compared to the reference situation. It is calculated with a 6th order polynomial regression function, whose input variables are the air temperature (T_a), the mean radiant temperature (T_{mrt}), the wind speed and the air relative humidity.

The method for the calculation of the mean radiant temperature is given by Eq. (9), from the International Standard ISO 7726:1998.

$$T_{mrt} = \sqrt[4]{(T_g + 273.15)^4 + \frac{1.06 \times 10^8 \times V_a^{0.58}}{\varepsilon \times D^{0.42}} \times (T_g - T_a)} - 273.15 \quad (9)$$

with T_{mrt} the mean radiant temperature (°C), T_g the globe temperature (°C), T_a the air temperature (°C), V_a the wind speed (m s^{-1}), ε the globe emissivity and D the globe diameter (m), respectively equal to 0.95 and to 0.15 m in the present study. Furthermore, the UTCI was estimated at the reduced-scale human height, *i.e.* 0.40 m a.g.l. corresponding to an actual full-scale height of 2.0 m, in both vegetated and non-vegetated street zones.

2.11. Studied periods

The studied period was defined from May 1, 2022, to September 14, 2022, and was divided into three periods *i.e.* from the beginning to trimming on June 23 (P1 period), from June 24 to the day before the beginning of the water restriction for WR alignment on July 5 (P2 period) and from July 6 to the end of the experiment (P3 period) (Fig. 2). A focus on the microclimatic data was carried out from May 13, 2022 to August 28, 2022.

Only sunny days, *i.e.* 42 days, were selected during this 108-day period, in order to analyze the maximum climate services provided by trees. These sunny days were defined by an insulation ratio (ratio of the daily integral of the global radiation reaching the top of street canyon site, over the daily integral of solar radiation above the atmosphere) higher than 0.65 as suggested by Mballo et al. (2021). On average over these 42 selected days, daily mean air temperature was 21.7 ± 0.09°C; daily minimum and maximum air temperatures were respectively 12.7 ± 0.52°C and 29.4 ± 0.69°C; daily air relative humidity was 52.4 ± 0.27 %; daily incident shortwaves radiation was 27.1 ± 0.36 MJ m^{-2} day^{-1}; and daily wind speed was 0.320 ± 0.0032 m s^{-1}. In the facility latitudes and given the street orientation, shade provided to pedestrians during solar noon could only be created by trees. Because the study focused on the pedestrian thermal comfort in a street canyon, the analyses were thus carried out over the solar noon period defined from 11:00 UTC to 13:00 UTC for sensors in the central axis of the street. This studied time frame was adapted from 12:40 UTC to 14:40 UTC for the sensors placed at 0.15 m from the east wall of the street canyon. The 1h40 offset corresponds to the additional time required for the east-side sensors to come out of the shade of the east wall in the morning. It was estimated by visual inspection of temporal evolution of globe temperatures in the NV zones, at the two positions. Within their respective temporal window of study, each set of sensors (on the center and on the east side) are then fully exposed to the sun in the NV zone, allowing to study by comparison the tree shading benefits in WW and WR zones.

2.12. Data processing

Data formatting, processing and statistical analysis were achieved

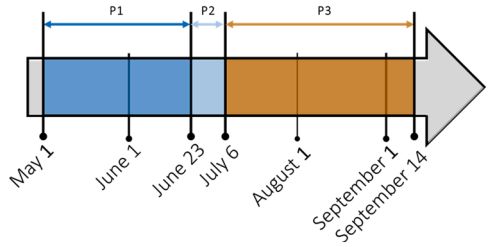

Fig. 2. Timeline of the whole studied period and its associated subdivisions. The P1 period was the pre-trimming period and P2 period lasted two weeks, referring to the post-trimming period. The P3 period referred to the period when differentiated water regime occurring between WW and WR tree alignments.

[1] The reference conditions are characterized by a wind speed of 0.5 m/s, a mean radiant temperature equal to the air temperature and a relative humidity of 50% (if air temperature < 29°C ; if not, water vapor pressure = 2 kPa) (Bröde et al., 2010).

using the RStudio software package, version 2023.9.1.494. Architectural data from June 6 and July 7 were respectively extrapolated to the days before and after trimming, to which were added and subtracted respectively data from measurements taken on the portions of axes removed by the trimming operation. More specifically, the total and defoliated lengths of the latter, and their leaf length and width, were used to obtain precise estimations for the length of axes and leaf area removed per tree by the trimming. Because of the time-consuming aspect of the ecophysiological measurements, architectural data were only available for 6 days during the whole period of study. Architectural variables at the tree alignment scale were then both linearly interpolated and extrapolated. To do so, the function *approxExtrap* from the *Hmisc* package was used.

Developmental data of the two tree alignments were assumed to be independent for all periods. Statistical comparisons at each measurement date were performed to study their architectural differences. Linear mixed models were used when several data of interest referred to a same tree. In this case, the measured tree was considered as a nested random effect, which was included behind the fixed effect of the tree alignment it belonged. Otherwise, classic linear models were applied to the data.

Either for a linear mixed model or a classic linear model, the parametric ANOVA test was used when the model residuals normality and their homoscedasticity were both verified. If not, data were subjected to the non-parametric Kruskal-Wallis test. The normal distribution of the model residuals was verified according to the Shapiro-Wilk test (and the Kolmogorov-Smirnov test in the same time). The homoscedasticity of the data was verified with the Bartlett test for classic linear models, and with the Levene test for linear mixed model. The angular distributions at each measurement date in WW and WR tree alignments were compared statistically using the Kolmogorov-Smirnov test. This test was also used to compare the angular distributions of the same alignment at two different dates.

Finally, tree transpiration, mean radiant temperature, and UTCI were computed using in-house Python 3 scripts already used in Thierry et al. (2024), and published in Herpin et al. (2024).

3. Results

3.1. Tree water status

The evolution of the trunks' micrometric diameter variations over the studied period shows that the radial growth rate of WW and WR trees was constant during P1 and P2 periods (Fig. 3A). Thus, the quantity of water supplied was sufficient to allow both the reconstitution of tree trunk's internal water storage each night and its secondary growth. During P3 period, WW trees exhibited continuous trunk radial growth, while the radial growth of WR trees nearly stopped from the 1st day of water restriction and showed daily trunk variation amplitudes higher than for WW trees. However, the internal water storage of WR trees was fully reconstituted from one day to the next, except between July 11 to July 18, when trees were watered only every other day.

On July 5 just before the differentiation of water supply between the two tree alignments, WW and WR tree alignments had similar $\Psi_{predawn}$ of −0.81 MPa and −0.84 MPa, respectively, indicating well-watered conditions (Fig. 3B). At this date and for the two tree alignments, $\Psi_{predawn}$ was higher than the Ψ_{stem}, which was itself higher than the Ψ_{leaf} (Fig. 3B and 3C). This logical arrangement between the three types of water potentials remained unchanged for trees in WW tree alignment all along P3 period. For WR trees, $\Psi_{predawn}$ was significantly more negative than the one of WW trees at each measurement date of P3 period. For a WR tree, $\Psi_{predawn}$ reached −3.39 MPa on July 19, before stabilizing around −1.38 MPa, while it remained around −0.41 MPa for a WW tree. At the beginning of the P3 period, we tested irrigation doses to reduce $\Psi_{predawn}$ in WR compared to WW, without decreasing trunk diameter. The significant drop in $\Psi_{predawn}$ on July 19 resulted from excessive dose

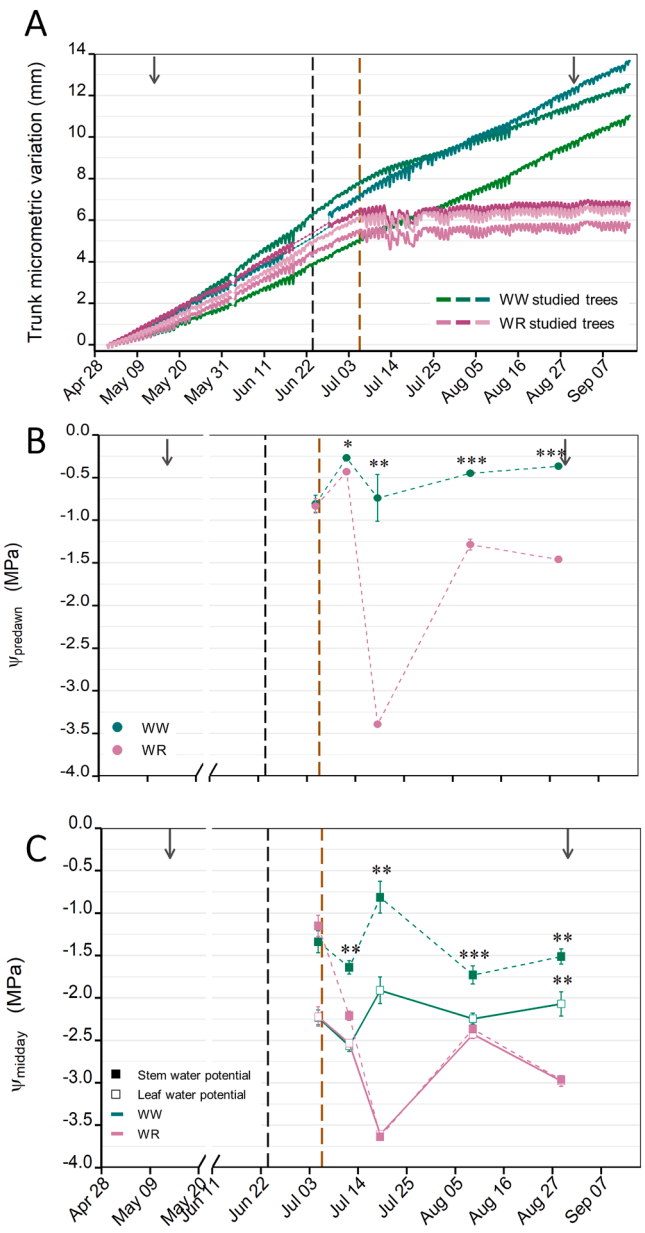

Fig. 3. Evolution of (A) the tree trunk micrometric variations, (B) the average predawn water potential and (C) both the average leaf (empty squares) and stem (full squares) water potentials at midday, for WW trees (green tones) and WR trees (pink tones). All micrometric curves were set to start from 0 mm on May 1, 2022. Vertical bars associated with water potentials represent ± the standard error. Symbols (*), (**) and (***) above predawn, leaf or stem water potentials denote significant differences between averages of each water potentials for WW trees and WR trees, respectively at $P < 0.05$, $P < 0.001$ and $P < 0.0001$ by ANOVA (11 times) or Kruskal-Wallis (4 times) test. The dotted black and orange vertical lines indicate the dates of trimming and start of water restriction (applied to WR trees), respectively. The two arrows indicate the beginning and the end of the bioclimatic studied period.

reduction due to irrigating every other day between July 12 and July 19, 2022. Resuming daily irrigation with a reduced dose starting July 20, 2022, stabilized the water potentials, as also indicated by consistent micro-dendrometric changes until the end of August. Stem water potential was lower for WR trees than for WW trees from the beginning of P3 period (Fig. 3C). During P3 period, Ψ_{leaf} and Ψ_{stem} were closer to one another for WR trees than they were for WW trees, indicating stomatal closure at midday for WR trees but not for WW trees.

Altogether these results indicate that during P1 and P2 periods, trees

in WW and WR alignments were not limited by water supply. During P3 period, water supply remained non-limiting for trees in WW alignment. In contrast and from the 1st day of P3 period, the limited apparent diameter growth of the trunk showed the limiting water supply for trees in WR alignment. Water restriction varied in intensity, but it remained globally moderate all along P3 period.

3.2. Architectural characterization of trees at crown scale

Both tree alignments were well watered during the P1 and P2 periods, and leaf area per tree almost doubled over P1 period for WW and WR tree alignments, reaching 4.61 m^2 and 4.40 m^2 per tree on June 22, respectively (Fig. 4A). The same trimming procedure was applied to all trees of the facility, reducing the leaf area per tree to 2.85 m^2 and 2.87 m^2 in WW and WR tree alignments, respectively, during P2 period. During P3 period, the leaf area of WW tree alignment, that remained in well-watered conditions, increased to 4.36 m^2 per tree by the end of P3 period on August 28. On the opposite, during water restriction imposed in P3 period to WR trees, their leaf area decreased by 41 %, reaching 1.70 m^2 per tree on August 28.

As shown in Fig. 4B, the PEA in WW and WR tree alignments more than doubled from May 1 during P1 period, reaching 11.1 m^2 and 10.7 m^2 respectively, by June 15. Together, they then covered nearly 70 % of the total surface area of the street canyon. Then, the PEA was nearly halved after trimming, and tree coverage dropped to just under 40 %. During the beginning of P3 period, the PEA increased by about 20 % and

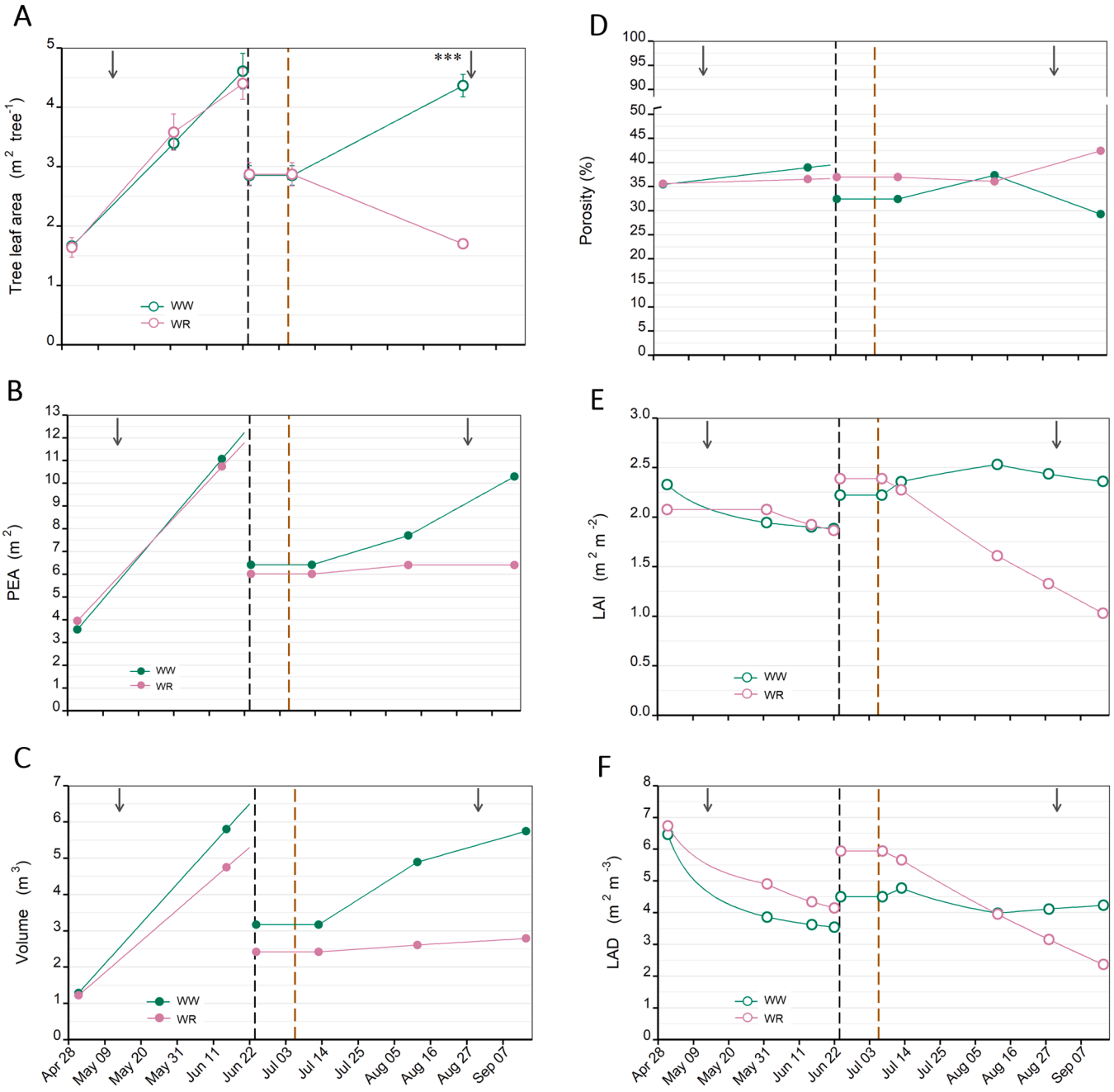

Fig. 4. Evolution of (A) the average leaf area per tree, (B) the projected area of the crown alignment envelope (PEA), (C) the volume of the crown alignment, (D) the porosity of the crown alignment, (E) the LAI and (F) the LAD, for WW trees (green) and WR trees (pink). Vertical bars represent ± the standard error. Symbol (***) denotes significant difference between averages at $P < 0.0001$ by ANOVA. The dotted black and orange vertical lines indicate the dates of trimming and start of water restriction (applied to WR trees), respectively. The two arrows indicate the beginning and the end of the bioclimatic studied period.

6.5 % until August 12 in WW and WR tree alignments, respectively. The difference between the PEA of the two tree alignments was most noticeable at the end of P3 period, as the PEA increased by about almost 34 % in WW tree alignment, while it remained unchanged in the WR tree alignment for the rest of P3 period. On September 14, the PEA reached 10.3 m^2 in WW tree alignment and only 6.4 m^2 in WR tree alignment which had been subjected to a moderate water restriction. As a result, tree coverage accounted for 53 % of the total surface area of the street canyon.

The crown volume strongly increased during P1 period for both WW and WR tree alignments (Fig. 4C). After trimming, the crown volume was nearly halved in both tree alignments. The crown volume of WW tree alignment increased at a faster rate at the beginning of P3 period than at the end, while under water restriction the crown volume of WR alignment remained almost stable throughout the entire P3 period. By September 14, the crown volume of WW tree alignment had nearly reached the level it was at the end of P1 period *i.e.* just before trimming, and it was twice as high as the crown volume of WR tree alignment.

Table 3
Crown architectural characteristics at organ scale (axis number and length, leaf number and area, and defoliation). Mean values ± standard error. Different letters at the same date indicate significant differences at $P < 0.05$, with lowercase letters denoting results from parametric statistical tests and capital letters denoting results from non-parametric ones.

		P1			P2	P3
	Studied alignment	May 1, 2022	June 1, 2022	June 22, 2022 (before trimming)	July 7, 2022 (after trimming and at the beginning of the water restriction)	August 28, 2022
G1 axis number per tree	WW	49.0 ± 1.1 ^{A}	53.7 ± 4.5 ^{A}	53.3 ± 5.5 ^{A}	53.3 ± 5.5 ^{A}	68.3 ± 4.7 ^{A}
	WR	58.7 ± 5.7 ^{B}	56.7 ± 3.5 ^{A}	53.3 ± 3.8 ^{A}	53.3 ± 3.8 ^{A}	60.0 ± 7.2 ^{A}
G2 axis number per tree	WW	-	-	-	-	46.7 ± 5.8 ^{a}
	WR	-	-	-	-	24.3 ± 1.2 ^{b}
G1 axis length (cm/axis) [1]	WW	28.2 ± 1.1 ^{A}	52.6 ± 2.6 ^{A}	46.4 ± 5.3 ^{a}	39.4 ± 2.9 ^{A}	39.4 ± 2.5 ^{A}
	WR	27.3 ± 1.1 ^{A}	53.7 ± 2.3 ^{A}	56.2 ± 4.9 ^{a}	42.9 ± 3.9 ^{A}	36.2 ± 2.9 ^{A}
G2 axis length (cm/axis)	WW	-	-	-	-	33.7 ± 2.5 ^{A}
	WR	-	-	-	-	1.28 ± 0.1 ^{B}
Leaf number per axis, for G1 axes [1]	WW	13.1 ± 0.5 ^{A}	20.3 ± 1.0 ^{A}	NA	15.9 ± 1.2 ^{A}	14.9 ± 0.9 ^{A}
	WR	13.2 ± 0.5 ^{A}	20.6 ± 0.9 ^{A}	NA	16.5 ± 1.1 ^{A}	13.0 ± 1.0 ^{A}
Leaf number per axis, for G2 axes	WW	-	-	-	-	17.0 ± 1.3 ^{A}
	WR	-	-	-	-	7.88 ± 0.9 ^{B}
Area of G1 long axis leaves (cm² / leaf) [1]	WW	19.2 ± 0.5 ^{A}	29.2 ± 0.5 ^{A}	NA	28.8 ± 0.5 ^{A}	26.3 ± 0.9 ^{A}
	WR	16.8 ±0.5 ^{B}	29.0 ± 0.5 ^{A}	NA	28.3 ± 0.5 ^{A}	32.8 ± 0.6 ^{B}
Area of G2 long axis leaves (cm² / leaf)	WW	-	-	-	-	20.6 ± 0.4 ^{A}
	WR	-	-	-	-	2.63 ± 0.1 ^{B}
Defoliation rate of the G1 axes (%) [1]	WW	0.20 ± 0.2 ^{A}	1.18 ± 0.9 ^{A}	3.69 ± 1.1 ^{A}	5.48 ± 1.5 ^{A}	26.0 ± 3.2 ^{A}
	WR	3.20 ± 3.1 ^{A}	0.38 ± 0.4 ^{A}	4.77 ± 0.6 ^{A}	6.56 ± 0.7 ^{A}	39.3 ± 2.2 ^{B}
Defoliation rate of the G2 axes (%)	WW	-	-	-	-	1.49 ± 0.6 ^{A}
	WR	-	-	-	-	3.83 ± 3.8 ^{A}

[1]On July 7 and August 28 only axes that remained untrimmed were included in the measurements, thus the population of G1 axes on which these measurements were performed was larger before than after trimming.

Despite large changes in leaf area, PEA and crown volume, crown porosity little changed between May 1 and August 12 in WW and WR tree alignments (Fig. 4D). By the end of P3 period, porosity diverged between WW and WR alignments, as it decreased by about 5 % points and increased by about 5 % points, respectively.

During P1 period, both tree alignments were well watered, and their LAI which was greater than 2.0 m^2 m^{-2} on May 1, slightly decreased to 1.9 m^2 m^{-2} on June 22 (Fig. 4E). After trimming, the LAI slightly increased to 2.2 m^2 m^{-2} and 2.4 m^2 m^{-2} in WW and WR tree alignments, respectively. Then, it slightly increased by 0.2 m^2 m^{-2} in WW tree alignment during P3 period, while under water restriction LAI strongly and regularly decreased from mid-July onwards in the WR tree alignment. It fell below 1.8 m^2 m^{-2} in early August and reach 1.3 m^2 m^{-2} by the end of P3 period.

While leaf area and crown volume increased, LAD decreased in WW and WR tree alignments during P1 period from 6.5 m^2 m^{-3} to <3.6 m^2 m^{-3} and from 6.7 m^2 m^{-3} to <4.3 m^2 m^{-3}, respectively (Fig. 4F). As a consequence of trimming, LAD increased and differed by 1.4 m^2 m^{-3} between WW and WR tree alignments during P2 period, corresponding to 4.5 m^2 m^{-3} and 5.9 m^2 m^{-3}, respectively. During P3 period, LAD slightly decreased in WW tree alignment whereas it markedly decreased by 3.6 m^2 m^{-3} in WR tree alignment until the end of P3 period.

3.3. *Architectural characterization of trees at organ level*

Architecture was characterized at organ scale to investigate the growth and developmental processes most involved in the evolution of crown architectural traits. The number of axes formed before trimming - G1 axes - remained almost stable throughout the experiment and was similar between the trees in the two alignments (Table 3). Small differences were observed between trees in the two alignments or between two measurement dates but these were likely due to observer bias, as identifying the type of axis could lead to confusion due to axis polymorphism and their stage of development. To study the characteristics of these G1 axes beyond their numbers, only untrimmed axes were considered. The reduced length of a G1 axis for both WW and WR trees after trimming indicates that trimming affected the longest axes. On average, the length of a G1 axis doubled during the P1 period, contributing to the increase in crown dimensions, and remained stable throughout the P3 period in both alignments. The number of leaves per G1 axes and their average area increased sharply during the P1 period, contributing to the significant increase in TLA in both the WW and WR alignments (Fig. 4A). The number of leaves and individual leaf area remained stable during P3 period on untrimmed G1 axes. Except for a 2 cm^2 difference in leaf area on May 1, there was no significant difference between the two alignments in terms of leaf number or area, regardless of the measurement date. This aligns with the fact that the alignments were exposed to different water conditions only during P3 period, when these traits were stable on untrimmed G1 axes. It is noteworthy that the untrimmed G1 axes were not the more vigorous, either visually or based on length measurements. Thus, if the vigorous axes had not been trimmed, their evolution in P3 could have been different from that of the population of untrimmed axes, as shown by the evolution of the G2 axes which took over from the trimmed G1 axes.

Trimming, by relieving apical dominance, induced the outgrowth of buds positioned immediately bellow the trimmed ends. At the beginning of P3, buds were already swollen, indicating that bud outgrowth was in progress. During P3, these buds developed in new – G2 – axes. Visual observation showed that bud outgrowth occurred only on vigorous axes that were still developing at the time of trimming, mostly located on the top of the crown. By the end of P3 period, the number of G2 axes was almost twice as high in WW trees as in WR trees. While G2 axes in the WR alignment elongated during P3, ensuring the increase in PEA and crown volume (Fig. 4B and 4C), their elongation was blocked to 1.3 cm by water restriction in WR tree alignment. Water restriction significantly reduced leaf number (8 leaves per axis in WR instead of 17 in WW) and individual leaf area (3 cm^2 per leaf in WR compared to 21 cm^2 in WW). It resulted in a TLA for G2 axes in the WR tree alignment of only 3 % of that in the WW tree alignment (0.05 m^2 *vs* 1.6 m^2).

Defoliation was measured as the relative length of the axes that had lost leaves. Defoliation remained very low and similar in the two tree alignments until the beginning of P3 period. Water restriction accelerated defoliation of the G1 axes, as at the end of P3 period it reached 39 % in WR tree alignment compared to 26 % in WW tree alignment. G2 axes were not affected by defoliation.

Fig. 5 shows that the leaves of trees in the two alignments were similarly oriented during P1 period ($P > 0.05$, both on May 5 and June 16). They were mostly pointing downwards with a median inclination angle which evolved from −37.2 ° and −28.8 ° to about +8 ° and +9 ° from the beginning to the end of P1 period for trees in WW and WR alignments, respectively (Table 2). At the end of P3 period, the inclination angles of the leaves borne on G1 axes and on G2 axes were quite different, as they did not account for the same proportion of the TLA (56.5 % and 34.5 % of the TLA, respectively). The leaves borne on G1 axes for trees in the two alignments showed a similar orientation again ($P > 0.05$). Contrary to May 5, this similar orientation extended over a range of inclination angles closer to a vertical, pointing downwards. The median inclination angle was more negative by about −11 ° for WW trees and −30 ° for WR trees. However, statistical analysis did not reveal significant differences between the angular distribution on May 5 and September 6 for the two tree alignments. In September, the area of a leaf borne by G2 axes of a WR tree represented on average only 8 % of the area of a leaf borne by G1 axes of the same WR tree, whereas the area of a G2 leaf of a WW tree was on average about 78 % of the area of a G1 leaf of the same WW tree. Therefore, only angular distribution of G2 leaves in WW alignment is shown. It was almost symmetrical around 0 ° with a median angle about +5 °, meaning that there was as many G2 leaves pointing downwards as leaves pointing upwards, and that the leaves were mostly horizontal.

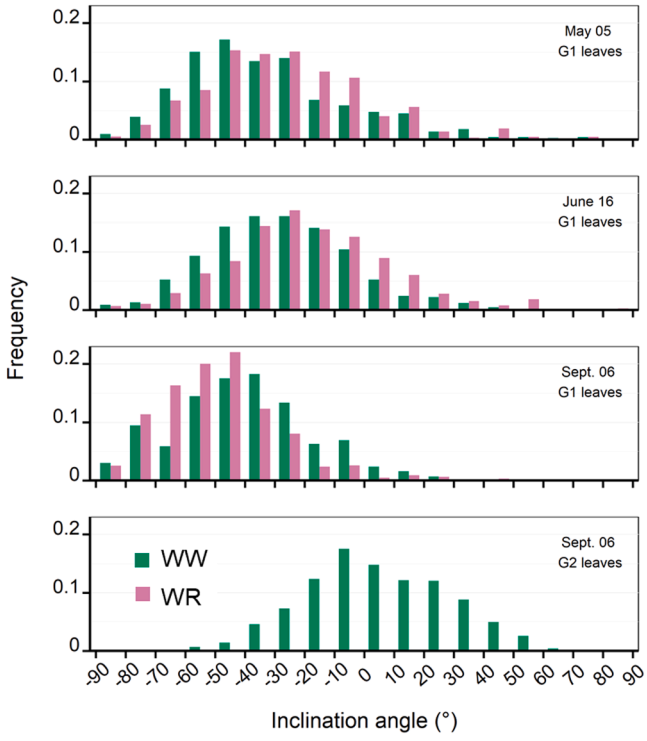

Fig. 5. Distribution of leaf inclination angle as a function of the leaf area frequency, for WW trees (green) and WR trees (pink).

3.4. Transpiration and light interception by tree alignments

During P1 period, transpiration for a tree in WW or WR alignment was on average similar (Fig. 6A). From May 1 to May 29, it increased in line with the leaf area, despite a quite stable ET_{ref} around 3.5 L m^{-2} day^{-1}. From June 1 until trimming, ET_{ref} increased and tree transpiration followed the same trend, in line with the increase in leaf area. During P2 period, tree transpiration was similar for trees in both alignments but lower than ET_{ref} and equaling tree transpiration observed in early June. At the beginning of P3 period, ET_{ref} remained fairly stable on selected sunny days, around 4 L m^{-2} day^{-1}, while transpiration was drastically reduced for WR trees. It was divided by almost 3 starting two days after water restriction began, and continued to gradually decrease throughout P3 period until it was nearly zero by August 28. In contrast, transpiration of WW trees was close to ET_{ref} and even exceeded it in early August. Since mid-August, it has slightly increased in line with the development of leaf area borne by their G2 axes.

During the whole studied period and regardless of the considered water treatment, the rate of intercepted short-wavelength radiation (*r ratio*) by a tree alignment was very high, comprised between 85 % and 95 % (Fig. 6B). During P1 and P2 periods, *r ratio* was quite similar between WW and WR tree alignments, with a <2 % points variation. On May 13, it was already higher than 87.5 % and then slightly increased. It often reached values exceeding 90 % from May 29, despite an important removal of leaf area due to trimming. From the beginning of P3 period to mid-July, the *r ratio* in WR tree alignment from now on under water restriction, slightly decreased whereas it slightly increased in WW tree alignment. This difference of light interception between WW and WR tree alignments did not exceed the maximum gap observed between the two tree alignments on June 16 when they were both well-watered.

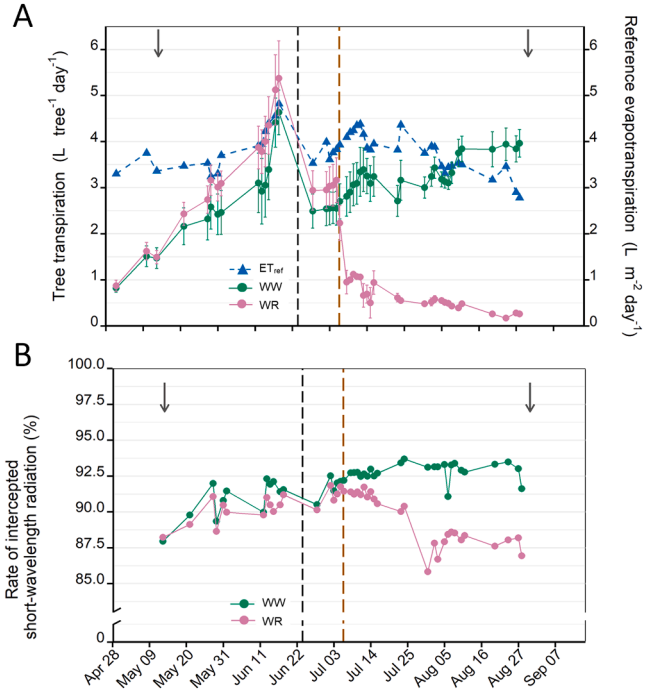

Fig. 6. Evolution of (A) the average transpiration per tree and (B) the rate of intercepted short-wavelength radiation between 11:00 UTC and 13:00 UTC on sunny days, for WW trees (green) and WR trees (pink). Blue triangle presents reference evapotranspiration of a studied day. Vertical bars represent ± the standard error. The dotted black and orange vertical lines indicate the dates of trimming and start of water restriction (applied to WR trees), respectively. The two arrows indicate the beginning and the end of the bioclimatic studied period.

From mid-July, this gap became higher. The *r ratio* in WR tree alignment decreased and stabilized in August just below values of May. After mid-July, the *r ratio* in WW tree alignment stabilized around 93 %. Differences between *r ratio* in WW and WR tree alignments reached up to 7 % points on July 31 and finally 5 % points on August 28.

Differences in transpiration and light interception between WW and WR tree alignments finally resulted from their respective crown architectural modifications described above. Also, P3 period could be divided into two periods for which the impacts on light interception did not appear to be of the same intensity.

3.5. Characterization of the UTCI as a function of microclimatic variables

As described in Section 2.10, the UTCI is a function of T_a, T_{mrt}, air relative humidity and wind speed. In this study, wind speed was assumed to be spatially homogeneously distributed at 0.40 m a.g.l. so the same measurement value was applied in the UTCI calculation. The greatest differences in air relative humidity between the NV and WW or WR tree alignment were about 2.1 % points, during solar noon periods, which cannot be considered as significant given the sensor accuracy (1.5 % points). Considering the averaged T_a range during the experiment and the psychrometric diagram presented by Bröde et al. (2010), it is concluded that the air relative humidity variations would not explain the UTCI variations during the studied period.

Differences of T_a at 0.40 m a.g.l. between NV zone and each tree alignment are presented in Fig. 7A and 7D, at the center and on the east side of the street respectively, and called from now on Delta(T_a). In the center of the street, the Delta(T_a) slightly increased over the whole studied period under WW tree alignment (Fig. 7A). This suggests a weak effect of architectural variations, whether natural or due to trimming, and a negligible impact of street T_a without trees, measured in the NV zone. Additionally, an average difference of about 1.0 ± 0.1°C was observed between the two Delta(T_a) associated with the two tree alignments, with the underside of WW tree alignment being cooler than that of the WR tree alignment throughout the studied period. This difference corresponded to a pre-existing discrepancy between the two TRH sensors. During P3 period, the air in the NV zone remained warmer than 27.5°C on the selected sunny days, but the difference between the two tree alignments hardly changed, and any change did not exceed the sensor accuracy of 0.2°C, despite the differentiated water treatment. The Delta(T_a) measured on the east side of the street followed the same trend (Fig. 7D), and were not affected by either trimming or water restriction applied to WR tree alignment during P3 period. A temperature difference between the WW and WR tree alignments was still observable and constant, but higher by about 1.7 ± 0.1°C on average than it was at the center of the street. This indicates that the WR zone was far warmer than the WW one on their east side all along the studied period. This may be linked to the greater canopy volume of the WW tree alignment and the proximity of the WR tree alignment to the NV zone, whose warmer air could have reached the sensor on the east side of the WR tree alignment.

Differences of T_{mrt} at 0.40 m a.g.l. between NV zone and each tree alignment are presented in Fig. 7B and 7E, at the center and on the east side of the street respectively, and called from now on Delta(T_{mrt}). At the center position, the Delta(T_{mrt}) were similar under the two tree alignments during P1 and P2 periods. It evolved from 16.1°C to 20.9°C and from 15.4°C to 19.8°C during P1 period, under WW and WR tree alignments, respectively (Fig. B). The Delta(T_{mrt}) was maintained around 20.5°C and 20.6°C during P2 period, under WW and WR tree alignments, respectively. During P3 period, Delta(T_{mrt}) hardly evolved under WW tree alignment. The Delta(T_{mrt}) remained close between the two tree alignments until mid-July. Then, the T_{mrt} became higher under WR tree alignment, resulting in a decrease of Delta(T_{mrt}) by about 3.0 ± 0.1°C on average during the rest of P3 period, compared to the beginning of P3 period. On the east side of the street, Delta(T_{mrt}) increased by about 9°C and 6°C during P1 period under WW and WR tree alignments, respectively. During this P1 period, it was on average 5°C higher when

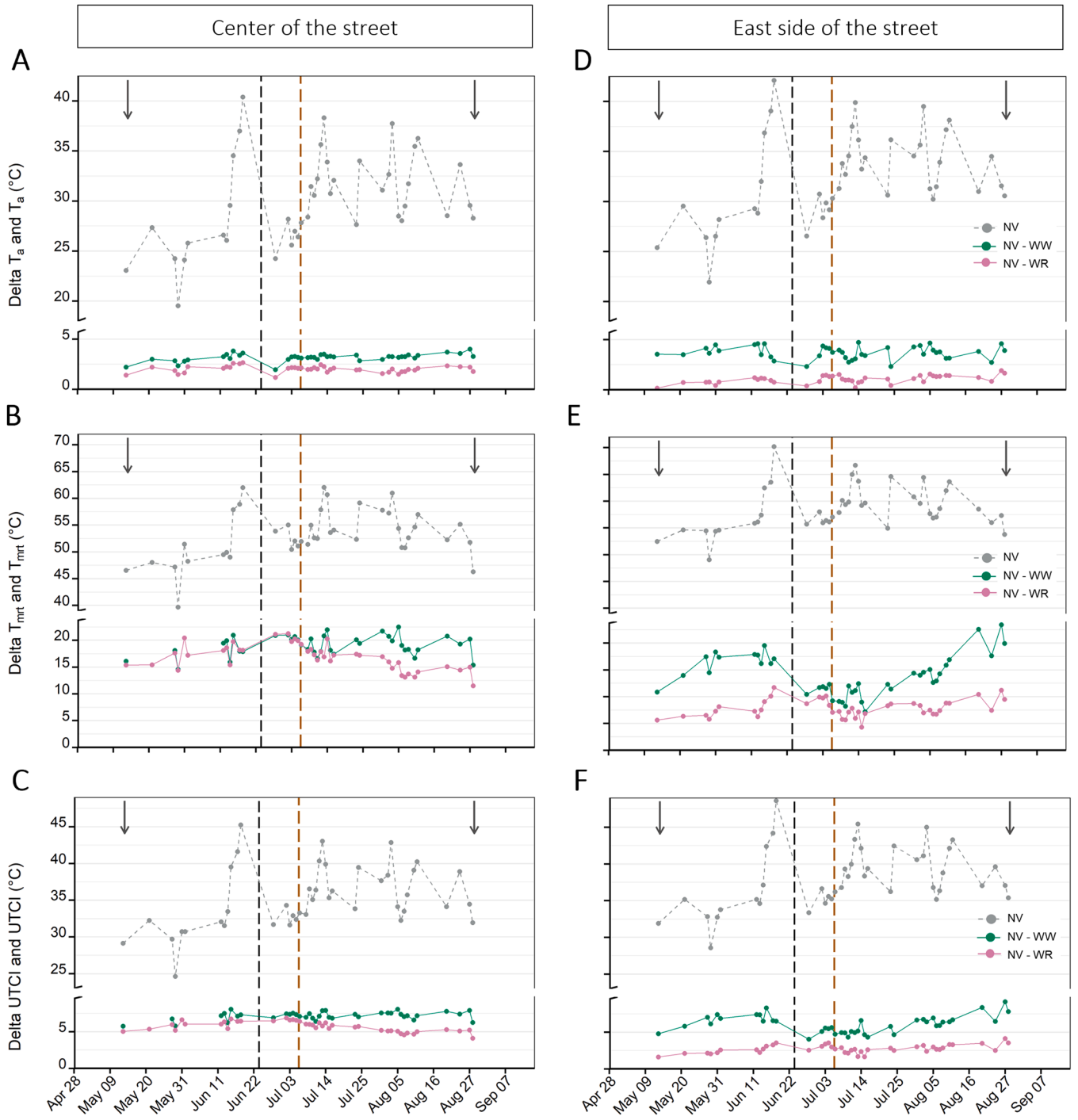

Fig. 7. Difference of (A) air temperature, (B) mean radiant temperature and (C) universal thermal climate index, between the NV zone (grey) and either WW (green) or WR tree alignment (pink), measured at 0.40 m above street level on sunny days in the center of the street. Difference of (D) air temperature, (E) mean radiant temperature and (F) universal thermal climate index, between the NV zone and either WW (green) or WR tree alignment (pink), measured at 0.40 m above street level on sunny days at the East side of the street. Grey points represent the associated variable measured in the NV zone at 0.40 m above street level on sunny days. The presented values have been averaged over solar noon, between 11:00 UTC and 13:00 UTC. The dotted black and orange vertical lines indicate the dates of trimming and start of water restriction (applied to WR trees), respectively. The two arrows indicate the beginning and the end of the bioclimatic studied period.

associated under WW tree alignment than under WR tree alignment (Fig. 7E). During P2 period, after trimming, T_{mrt} was almost identical under both tree alignments, and Delta(T_{mrt}) remained stable around 11.6°C and 9.4°C under WW and WR tree alignments, respectively. Given that wind speed data used in the T_{mrt} calculation were the same for the two tree alignments and that T_a remained almost stable during P1 period, this suggests that the globe temperature was involved in such variations of T_{mrt} between the two tree alignments (Fig. 8). From the beginning of P3 period to mid-July, Delta(T_{mrt}) were stable on the east side in the two tree alignments. For the rest of P3 period, Delta(T_{mrt}) kept almost stable in WR tree alignment, whereas it had more than doubled in WW tree alignment.

Differences in UTCI at 0.40 m a.g.l. between NV zone and each tree alignment are shown in Fig. 7C and 7F, for the center and east side of the street, respectively, and will henceforth be referred to as Delta(UTCI). During P1 period at the center position, Delta(UTCI) evolved from 5.8°C

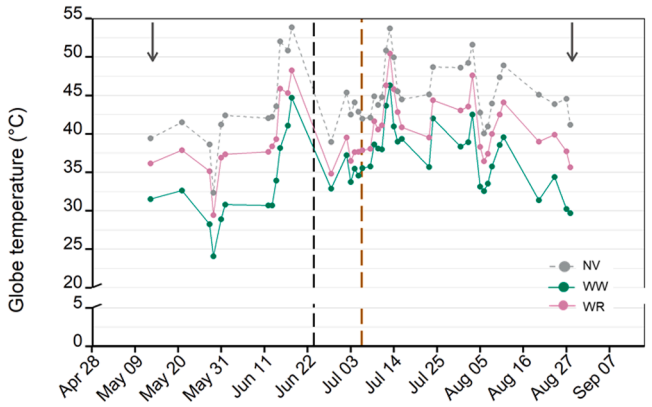

Fig. 8. Globe temperature measured at 0.40 m a.g.l. on sunny days on the east side of the street, for WW alignment (green), WR alignment (pink) and NV zone (grey). The dotted black and orange vertical lines indicate the dates of trimming and the start of water restriction (applied to WR trees), respectively. The two arrows indicate the beginning and the end of the bioclimatic studied period.

to 8.1°C under WW tree alignment and from 5.0°C to 6.7°C under WR tree alignments (Fig. 7C). Trimming did not impact UTCI at the center of the street as during P2 period, Delta(UTCI) remained almost constant and equal to 7.3 ± 0.1°C and 6.6 ± 0.1°C on average in WW and WR tree alignments, respectively. From the beginning of P3 period to mid-July, Delta(UTCI) hardly expanded to 1.2 ± 0.1°C on average in the two tree alignments. After mid-July, UTCI increased in WR tree alignment and the associated Delta(UTCI) decreased on average by about 0.9 ± 0.1°C compared to the beginning of P3 period, whereas it remained constant in WW tree alignment. On the east side of the street, Delta (UTCI) was higher by about 4.2 ± 0.2°C on average in WW tree alignment than in WR tree alignment during P1 period (Fig. 8F). After trimming, these differences were reduced but Delta(UTCI) in WW tree alignment was still higher than in WR tree alignment by about 2.0 ± 0.2°C. From the beginning of P3 period to mid-July, Delta(UTCI) differed between the two tree alignments as they did during P2 period. For the rest of P3 period, Delta(UTCI) hardly changed in WR tree alignment whereas it increased by about 1.7 ± 0.3°C on average in WW tree alignment. In both center and east studied positions, the trends of Delta(UTCI) in the two tree alignments were similar to the T_{mrt} ones.

4. Discussion

In the present study, we focused on sunny days which were defined according to the insulation ratio. This selection disclosed restrictive range of radiation variability, meaning the climate services were rather related to the trees than to meteorological condition variations. Summer 2022 was characterized by relatively hot weather conditions in Angers, France: strong and very strong heat stress ($32°C \leq$ UTCI $< 46°C$ according to Bröde et al. (2012)) levels were reached in the NV zone on 40 days over the 42 selected days.

The evolution of the architectural modifications of WW and WR tree alignments of *Malus Coccinella*® 'Courtarou' was presented over the 2022 growing season. Major architectural changes occurred at both organ and crown scales at the beginning of the growing season and just after trimming, when both tree alignments were well watered. During these two periods, TLA, PEA and crown volume increased markedly, driven by a substantial stem elongation and leaf expansion. At the same time, LAI showed little variation, and LAD decreased. At the beginning of P1 period, tree transpiration in both alignments followed the dynamics of TLA, and light interception slightly increased. At the same time, Delta(T_a), Delta(T_{mrt}) and Delta(UTCI) at the central position increased by 1.2°C, 4.4°C and 1.4°C, respectively. Transpiration and Delta(T_a) evolved after trimming when Delta(T_{mrt}) and Delta(UTCI) stabilized at the central position of the street.

The architectural evolution was then compared between the two tree alignments after water restriction started in the WR alignment. The dynamics of transpiration of WW trees was influenced both by their TLA development and by ET_{ref}, whereas transpiration was drastically reduced from the beginning of the water restriction for WR trees. Large increases in TLA, PEA and crown volume in WW led to a slight increase in the *r ratio*, while a decrease was observed in WR. Finally, T_a, T_{mrt} and UTCI evolved differently over time and space depending on the tree alignment. Delta(UTCI) remained stable under WW tree alignment, whereas it decreased under WR tree alignment at the center of the street during P3 period, with a maximum difference of 2.7°C between the two alignments. On the east side of the street, climate services were more variable than in the center over the growing season, regardless of tree alignment. To go further in the analysis, the following discussion focuses on the implication of tree architectural modifications in the evolution of climate services during a growing season. A discussion dealing with the effects of a water restriction on architectural modifications and their consequences on climate services is also provided.

4.1. How do architectural changes of well-watered trees influence their climate services throughout a growing season?

We focus here on well-watered trees, *i.e.* on WW and WR tree alignments during P1 and P2 periods and WW tree alignment during P3 period. During these periods, the evolution of tree transpiration followed that of TLA, modulated by the evolution of ET_{ref}. Tree transpiration probably contributed to the evolution of Delta(T_a), previously defined as the difference of T_a at 0.40 m a.g.l. between NV zone and under a tree alignment. However, this contribution appeared to be limited as the evolution of Delta(T_a) did not follow that of tree transpiration. Tree transpiration was <1.0 L tree^{-1} day^{-1} when Delta(T_a) was already about 1.8°C on May 13, at the beginning of P1 period on average for WW and WR tree alignments. Then, Delta(T_a) slightly increased, by 1.4°C on average, to reach a value of 2.2°C, during P1 period when tree transpiration strongly increased, by 3.5 L tree^{-1} day^{-1}. In comparison, Sharmin et al. (2023) reported that T_a was reduced by up to 3.7°C at 1.50 m a.g.l. under tree shade, in a full-scale street. Moreover, the evolution of Delta(T_a) was similar under WW and WR tree alignments over a period covering the last 4 sunny days of P2 period and the first 4 sunny days of P3 period. Yet, transpiration abruptly decreased by 2.3 L tree^{-1} day^{-1} the first days of P3 period for WR trees, following the beginning of water restriction, while it slightly increased for WW trees. This indicates that transpiration little contributed to the benefits in T_a provided by WW trees at that time. These results are consistent with other studies underlying the low contribution of transpiration to climates services provided by *Malus Coccinella*, but also by *Robinia pseudoacacia* L. and *Tilia cordata* Mill., particularly at pedestrian height where the effects of tree transpiration are less important than at crown height (Mballo et al., 2021; Rahman et al., 2018, 2020; Thierry et al., 2024).

At the beginning of P1 period, Delta(UTCI) and Delta(T_{mrt}) were already about 5.8°C and 15.4°C under WW tree alignment, respectively. This resulted from a *r ratio* that was already higher than 87 %. It was due to the fact that almost all G1 axes were already present, partly elongated and bearing expanding leaves. Kong et al. (2017) associated T_{mrt} reductions to *r ratio* measurements under canopies of different tree species and focused on the whole daytime. They found a T_{mrt} reduction of 3.8°C associated with a *r ratio* of 74 % for the deciduous *Peltophorum pterocarpum*. The work of Huang et al. (2020) aimed to measure changes in microclimate parameters as T_{mrt} under different street tree canopy covers subjected to the temperate climate in Wuhan, China. In a street with an aspect ratio of $H/W = 0.61$, they measured a 13.9°C T_{mrt} reduction under a dense tree canopy at solar noon (12:00 UTC to 14:00 UTC), characterized by a tree cover ratio of about 94 %. However, the evolution of the relationship between T_{mrt} and *r ratio* over the whole growing season had not been investigated until the present study.

During P1 period, Delta(T_{mrt}) and Delta(UTCI) under the WW tree alignment increased in the center of the street by +4.4°C and +1.5°C, respectively, and also rose on the east side of the street by +8.7°C and +3.5°C, respectively. The evolution of Delta(UTCI) resulted from the evolution of both Delta(T_a) and Delta(T_{mrt}) (Fig. 7A and 7B). The latter showed the importance of tree cast-shadow in the improvement of HTC, as cast-shadow affects the radiative environment on which T_{mrt} mainly relies. In the present study, the increase of Delta(T_{mrt}) in the central position was probably mostly explained by the slight increase and then the stabilization of the *r ratio* above 90 % in the two tree alignments during P1 period, when strong architectural modifications occurred. Indeed, the crown spatial dimensions of WW and WR tree alignments changed as their PEA and their volume increased (by at least +6.7 m^2 and +3.5 m^3) between the beginning and end of P1 period, resulting from the elongation of G1 axes. It meant the lower part of the street was increasingly overhung by the tree canopy and the lateral walls were increasingly shaded over P1 period, which certainly reduced the reflection of short-wavelength radiation by the building white walls towards the radiometers below the canopies. Thus, the crown spatial dimensions could explain the slight increase of the *r ratio* during the first month of P1 period when LAI was already higher than 2.0 $m^2\ m^{-2}$. Yet, the LAI and LAD decreased from 2.2 to 1.9 $m^2\ m^{-2}$, and from 6.6 to 4.0 $m^2\ m^{-3}$, respectively (and on average for the two tree alignments). The slight decrease of LAI however did not reduce climate services during P1 period, and the minimal value of 1.8 $m^2\ m^{-2}$ could thus be a threshold value of LAI for *Malus Coccinella*® 'Courtarou' to ensure a r ratio of 87 %. The existence of such threshold value of LAI is consistent with the conclusions of Rahman et al. (2019), indicating that when LAI was higher than a certain value, it was no longer correlated to surface temperature. This is all the more relevant that this conclusion was obtained on both *Robinia pseudoacacia* L. and *Tilia cordata* Mill. Also, Sanusi et al. (2017) found that PAI from three species inside three similar *in-situ* street canyons were on average different, whereas their associated PET reductions were not significantly different. The PAI of *Eucalyptus scoparia* was about 2.6 $m^2\ m^{-2}$ and its human thermal comfort improvement by about 4.76°C, *i.e.* only 0.5°C smaller than the one associated to *Ulmus procera* whose PAI equaled 5.9 $m^2\ m^{-2}$. Using sensitivity analysis, Chen et al. (2023) showed that increasing LAI reduced UTCI but that a plateau was reached above a threshold of LAI. In their conditions the plateau was due to a balance between effects favorable to thermal comfort on T_{mrt} and unfavorable to thermal comfort on relative humidity and wind speed, showing the complexity of the relationships. However, they did not investigate the relationship with *r ratio*.

During P2 period, the *r ratio* was not reduced compared to P1, probably because the reductions in PEA and volume caused by trimming were offset by LAI and LAD which remained above the aforementioned thresholds.

During P3 period, WW tree alignment was still well-watered and the development of new axes following trimming strongly modified its architecture. However, climate services did not evolve at the center of the street as canopy density remained high enough to maintain the maximal *r ratio*. Also, the horizontality of G2 leaves compared with G1 leaves could explain the increase of *r ratio* from the 2nd part of P3 period, and could be one of the reasons why it remained above 92.5 % (Figs. 5 and 6B). Despite the slight increase of the LAI and the slight decrease of LAD, Delta(UTCI) was not affected at the center of the street. Yet, Delta(UTCI) on the east side of the street increased from July 16, *i.e.* from the beginning of the 2nd part of P3 period. This could be hardly linked to the changes of the *r ratio,* as it increased only slightly. It was most likely due to an increase of tree cast shadows on this side of the street, since the climate services on the east side of the street were measured between 12:40 UTC and 14:40 UTC (just after the influence of morning shade from the east wall has ceased). The increase in tree cast-shadow on the east side of the street was driven by the PEA and the volume of WW tree alignment that increased throughout P3 period, with crown volume increasing more rapidly during the 1st part of P3 period, and PEA growing at a faster rate during the 2nd part of the period.

All things considered, the results show climate services provided by a WW tree alignment remained largely ensured along the growing season as long as the indicators of canopy density remained above certain thresholds. Then, these climate services were enhanced spatially, as strong architectural development led to an expansion of the crown spatial dimensions. Transpiration seemed to have small contribution to climate services at human height because transpiration occurs at crown height, and undergoes a faster dissipation of the cooling effect due to mixing with the surrounding air. The effects of cast-shadow are then much more lasting (Armson et al., 2012).

4.2. How does water restriction impact tree climate services?

During P3 period, 25 days had an insulation ratio above 0.65 and they presented an important climatic demand as shown by ET_{ref} (Fig. 6A). Thus, the water restriction was all the more relevant that it coupled an edaphic drought to high ET_{ref}, as frequently found in cities. Water restriction was applied to the tree alignment positioned in the middle of the street, *i.e.* to WR tree alignment. The different architectural and ecophysiological traits displayed either small or non-significant differences (when statistically comparable) between the two tree alignments over P1 and P2 periods. Thus, architectural and ecophysiological differences between WW and WR tree alignments during P3 period can be attributed to the effects of the water treatment rather than to an effect of the location of the tree alignment within the street.

From the beginning of P3 period to mid-July *i.e.* during the 1st part of P3 period, the transpiration of WR trees was drastically reduced by more than a factor 3 on average (Fig. 6A). During these first two weeks of water restriction for WR alignment, visual observations showed that future G2 axes were limited to swollen buds with no separated or expanded leaf. Additionally, the inclination angle of G1 leaves in WR alignment was not affected by the water treatment, even after prolonged water restriction. This is noteworthy because for other species, it could have rapidly varied due to a reduced turgor pressure from the decreasing leaf water potential. Thus, it was assumed that no major variation in architecture had occurred from July 6 to July 16, or that any variations were quite minor given that the *r ratio* only slightly decreased during these days. The *r ratio* remained higher than 90 % and was thus sufficient to provide enough cast-shadow to ensure the same level of climate services, as already evidenced by Thierry et al. (2024). This analysis supported the findings from Section 4.1 according to which cast-shadow plays a major role in the evolution of climate services compared to transpiration, especially when trees are water limited, an aspect still little explored in previous studies.

From July 23 to the end of P3 period *i.e.* during the 2nd part of P3 period, the *r ratio* decreased and stabilized around 87.5 % for WR tree alignment. The difference of *r ratio* between WW and WR tree alignments increased. It was influenced by architectural modifications of WR trees, resulting in a variation in shading effects and thus in variations of Delta(T_{mrt}) and Delta(UTCI). These variations were more or less important depending on whether they were calculated at the center or on the east side of the street. At the center of the street, the difference of climate services due to cast-shadow between the two tree alignments was rather due to reduction of canopy density in WR tree alignment compared to WW tree alignment. The defoliation of WR trees led to a loss of TLA that was not offset by the development of new axes and their PEA and volume slightly increased. This led LAI and LAD to fall below their lowest values reached during P1 period and could explain the decrease of the *r ratio* at the center of the street. It went along with a quite slight decrease of Delta(T_{mrt}) and Delta(UTCI) calculated under the WR canopy at the center of the street (Fig. 7B and 7C). Yet, at the same time, Delta(UTCI) on the east side of the street was kept stable, while it almost doubled for WW tree alignment (Fig. 7E and 7F). These observations support the conclusion that canopy dimensions had a key

role in maintaining climate services on the east side of the street, especially since PEA and crown volume in WR tree alignment remained relatively stable. Additionally, the leaves borne on G1 axes had become more vertical by the end of P3 period, allowing for greater interception of westerly solar radiation. This led in a reduction in the amount of radiation reaching the east side of the street.

These results help understand the effects of an edaphic drought on tree development and their consequences on climate services. The application of a prolonged water restriction led to notable differences in climate services between WW and WR tree alignments. These differences became more pronounced during the 2nd part of the water restriction period. They were mainly attributed to a reduction in transpiration, a decline in LAI below the threshold required to maintain an optimal *r ratio*, and changes in crown dimensions. Transpiration of WR trees was affected throughout the whole water-restricted period, but its effect on thermal comfort at the pedestrian level remained moderate, as already mentioned in Thierry et al. (2024). The LAI decreased and was no longer sufficient to ensure high light interception by WR canopy in the center of the street. As WR canopy density decreased, the near-stability of Delta(UTCI) at the east of the street could thus be only attributed to the stability of crown dimensions. Thus, the differences in climatic services between the two tree alignments due to architectural modifications could be explained both by the defoliation of WR trees (at the center of the street) and by the stop of the axis development (at the east side of the street). Yet, the extent to which tree climate services are affected may vary depending on the intensity and type of droughts. As shown by Chen et al. (2024), the transpiration of *Pinus sylvestris* var. mongolica in a semi-arid climate was significantly reduced during a combined atmospheric and edaphic drought, and even more so during an edaphic drought.

4.3. Implications of architectural traits in tree climate services

This study emphasized the importance of a sufficient LAI for ensuring high short-wavelength radiation interception levels, which significantly improved thermal comfort (characterized by a high Delta(UTCI)) under WW tree alignment from May to August. The bud outgrowth phase at the start of the season was crucial for producing an adequate number of axes, as the number of G1 axes remained stable from May onward. The increase in crown dimensions depends on axis elongation. The latter must be coupled with adequate leaf emission and blade expansion to maintain a LAI above the threshold enabling maximum interception, since increased crown dimensions were associated with reduction in LAI. Therefore, the sensitivity of the tree species to the different conditions that may delay or impair bud outgrowth, leaf initiation, stem and leaf expansion should be analyzed when choosing species, particularly in the perspective of climate change. For instance, insufficient winter chill can delay or impair bud outgrowth in various species and reduce new shoot growth, which could, in view to the present results, have an impact on climate services for a long part of the season (Asse et al., 2018; Man et al., 2021; Pletsers et al., 2015).

Studies quantifying the loss of climate services due to drought are still rare and often focus on tree transpiration losses (Drake et al., 2018; Rahman et al., 2024; Rötzer et al., 2021). Shashua-Bar et al. (2023) and Thierry et al. (2024) highlighted the major role of cast-shadow effects in provided climate services under drought conditions in hot arid or temperate climate. The present study builds upon this by demonstrating that drought mainly reduced climate benefits through its impact on tree architecture, which in turn affected cast-shadow effects. Nevertheless, the loss in climate services remained moderate under the imposed moderate water restriction, with Delta(UTCI) at the center of the street decreasing by 2.7°C under WR tree alignment compared to WW tree alignment in late August, representing a 34 % reduction.

If a water restriction was to occur in early spring, the effects on services would probably be greater as they would apply to trees with smaller leaf area and crown dimensions. These effects could be even more pronounced if the restriction coincided with the bud outgrowth period. Tree architectural responses to drought are not largely documented but concern many species, with interactions between species, water conditions and other factors such as tree class age (Liu et al., 2022). Understanding tree architectural plasticity in response to drought is therefore essential for selecting species suited to local water conditions, in order to maintain high levels of climate services. Architectural plasticity in response to drought should also be accounted for when modeling tree climate services.

Trimming significantly affected tree development and thus tree architecture. It was performed to align trees with street dimensions. While infrequent during the growing season in temperate climates, such trimming is sometimes carried out in cities. Predicting the impact of architectural changes without trimming remains challenging. At the onset of water restriction, LAI would likely have been lower, while PEA and crown volume would have been higher. Assuming similar ecophysiological responses to drought, the arrest development of G1 axes would have halted the evolution of PEA and crown volume, and prevented the development of new leaves. Additionally, defoliation of previously formed leaves would have further reduced LAI. As a result, climate services may have been more impaired in the center of the street (due to lower LAI) and less impaired on the east side (due to higher PEA and crown volume), compared to the effects observed with trimming. *Tilia sp* in French and English urban parks subjected to thinning or pruning, either in summer or in autumn, develop a higher LAI and thus higher shading and evaporating cooling effects (Ngao et al., 2021). Trees were not subjected to water restriction and the authors suggested that tree management could improve thermal comfort through its consequence on tree architectural development.

5. Conclusions

The present study was conducted to assess whether architectural modifications to urban trees during the growing season and water restrictions contribute significantly to variations in the climatic services provided by ornamental apple trees grown inside a reduced-scale street canyon

Under optimal growing conditions, the trees grew rapidly but exhibited vertical crown spread. The combined effect of shading and transpiration increased the benefit on HTC under the trees (UTCI reduction of 6.3°C on average, compared with the non-vegetated zone) and reduced air temperature under the trees (by 2.6°C on average) and T_{mrt} (by 17.6°C on average). Under well-watered conditions, modifying tree architecture (trimming) had no effect on the rate of intercepted short-wavelength radiation by the tree alignment but significantly impacted tree transpiration (40 % reduction). The climate services provided by the trees were maintained (2.4°C reduction in T_a, 20.5°C reduction in T_{mrt}, and 7.0°C reduction in UTCI compared with the non-vegetated zone). Water restriction also affected climate services provided by trees (an average increase in T_{mrt} of about 3.2°C and a resulting 1.9°C increase in UTCI compared with well-watered trees). Tree architectural modifications, by inhibiting stem growth and accelerating leaf fall, along with a strong reduction in transpiration, which was close to zero, were observed. By comparing these two situations, our findings support that thermal comfort is mainly linked to the architectural development of the trees, and to shade rather than to transpiration.

The knowledge of the seasonal variability of tree architecture induced by anthropic (trimming) or climatic (drought) events and associated climate services could help enhance urban planning and policies guidelines. It particularly addresses the importance of considering the conditions in which trees are planted as they significantly influence the tree long-term growth. This work provides some elements by showing how the lack of water may affect climate services through architectural effects, but it remains quite specific with respect to a tree species and a timing of trimming and water restrictions. This work should be complemented by further experiments to explore such timing

effect in more depth in relation to the phenology of tree species. Finally, and beyond the specific scientific questions underlying this work, another asset of this study was the number of collected data on the interactions between tree architecture and climate services both in well-watered and water-restricted conditions, that constitutes a unique and useful dataset to test and improve models linking tree architecture, light interception, and climate services.

Funding

This work was funded by the French Region Pays de la Loire and the French Ministry of Education, Research and Innovation through a Contrat de Plan Etat-Région (CPER). This research was conducted in the framework of the regional program "Objectif Végétal, Research, Education and Innovation in Pays de la Loire", supported by the French Region Pays de la Loire, Angers Loire Métropole and the European Regional Development Fund.

Declaration of generative AI and AI-assisted technologies in the writing process

During the preparation of this work the authors used DeepL and ChatGPT in order to improve the readability and language of the manuscript. After using this tool/service, the authors reviewed and edited the content as needed and take full responsibility for the content of the published article.

CRediT authorship contribution statement

Dorine Canonne: Writing – review & editing, Writing – original draft, Visualization, Validation, Software, Methodology, Investigation, Formal analysis, Data curation, Conceptualization. **Sophie Herpin:** Writing – review & editing, Validation, Supervision, Software, Project administration, Methodology, Funding acquisition, Formal analysis, Data curation, Conceptualization. **Julien Thierry:** Writing – review & editing, Software, Investigation, Data curation. **Camille Le Bras:** Software, Investigation. **Bénédicte Dubuc:** Methodology, Investigation. **Lydie Ledroit:** Investigation, Data curation. **Denis Cesbron:** Investigation, Data curation. **Marc Saudreau:** Writing – review & editing, Validation, Supervision, Software, Project administration, Methodology, Funding acquisition, Formal analysis, Data curation, Conceptualization. **Pierre-Emmanuel Bournet:** Writing – review & editing, Validation, Supervision, Project administration, Methodology, Funding acquisition, Formal analysis, Conceptualization. **Sabine Demotes-Mainard:** Writing – review & editing, Validation, Supervision, Project administration, Methodology, Funding acquisition, Formal analysis, Data curation, Conceptualization.

Declaration of competing interest

The authors declare that they have no known competing financial interests or personal relationships that could have appeared to influence the work reported in this paper.

Acknowledgements

We thank Rachel Levi (EPHor, Institut Agro Rennes-Angers and Université de Lyon, France) for her investment in the experimental investigation during her internship. Our warmly thanks go to Lydia Brialix (EPHor, Institut Agro Rennes-Angers, France) for her help in the architectural measurement campaigns, and for the bioclimatic instrumentation and maintenance with Dominique Lemesle (EPHor, Institut Agro Rennes-Angers, France). We thank Patrice Cannavo (EPHor, Institut Agro Rennes-Angers, France) for his advices regarding soil materials and analyses, and Soulaiman Sakr (Univ Angers, Institut Agro, INRAE, UMR IRHS) for his contribution to the initial conceptualization of this research project and fruitful discussion. Yvette Barraud-Roussel (EPHor, Institut Agro Rennes-Angers, France) is also thanked for the establishment of the experimental water retention curve used for the soil characterization. We then thank Cyril Bozonnet (PIAF, Clermont-Ferrand, France) for providing TLS data using the MatLab script, and Ronghai Hu (University of Chinese Academy of Science, Beijing, China) for his advices on the use of his PATH-model. Our thanks also go to Johann Kraft and Louison Bousselat (interns IRHS from Univ Angers, France) for their support in foliar digitizing and pre-processing of the TLS data, respectively. Pierre Santagostini (Univ Angers, Institut Agro, INRAE, UMR IRHS) is thanked for his statistical analysis advices. This experiment was conducted on the PHENOTIC platform (DOI: 10.17180/ykbz-2v85), and we thank the staff of PHENOTIC for their support in maintaining the experiment. We also thank the André Briant Jeunes Plants nursery (Saint-Barthélemy-d'Anjou, France) for supplying the trees. This work was carried out as part of the research contract between INRAE and Institut Agro dated 20 December 2021, agreement 3891.

Data availability

Data will be made available after a period of two years from the date of publication of the article, to enable to complete the analysis of the entire dataset.

References

Akbari, H., Pomerantz, M., Taha, H., 2001. Cool surfaces and shade trees to reduce energy use and improve air quality in urban areas. Sol. Energy 70 (3), 295310. https://doi.org/10.1016/S0038-092X(00)00089-X.

Allen, R.G., Pereira, L.S., Raes, D., & Smith, M. (1998). Crop evapotranspiration, guidelines for computing crop water requirements, FAO irrigation and drainage paper. FAO Irrigation and Drainage Paper.

Arifwidodo, S.D., Chandrasiri, O., 2020. Urban heat stress and human health in Bangkok, Thailand. Environ. Res. 185, 109398. https://doi.org/10.1016/j.envres.2020.109398.

Armson, D., Stringer, P., Ennos, A.R., 2012. The effect of tree shade and grass on surface and globe temperatures in an urban area. Urban For. Urban Green. 11 (3), 245255. https://doi.org/10.1016/j.ufug.2012.05.002.

Asse, D., Chuine, I., Vitasse, Y., Yoccoz, N.G., Delpierre, N., Badeau, V., Delestrade, A., Randin, C.F., 2018. Warmer winters reduce the advance of tree spring phenology induced by warmer springs in the Alps. Agric. For. Meteorol. 252, 220230. https://doi.org/10.1016/j.agrformet.2018.01.030.

Baïram, E., Delaire, M., Le Morvan, C., Buck-Sorlin, G., 2017. Models for predicting the architecture of different shoot types in Apple. Front. Plant Sci. 8. https://doi.org/10.3389/fpls.2017.00065.

Ballester, C., Buesa, I., Bonet, L., Intrigliolo, D.S., 2014. Usefulness of stem dendrometers as continuous indicator of loquat trees water status. Agric. Water Manage 142, 110114. https://doi.org/10.1016/j.agwat.2014.04.019.

Barthélémy, D., Caraglio, Y., 2007. Plant architecture : a dynamic, multilevel and comprehensive approach to Plant form, structure and ontogeny. Ann. Bot. 99 (3), 375407. https://doi.org/10.1093/aob/mcl260.

Blazejczyk, K., Epstein, Y., Jendritzky, G., Staiger, H., Tinz, B., 2012. Comparison of UTCI to selected thermal indices. Int. J. Biometeorol. 56 (3), 515535. https://doi.org/10.1007/s00484-011-0453-2.

Bowler, D.E., Buyung-Ali, L., Knight, T.M., Pullin, A.S., 2010. Urban greening to cool towns and cities : a systematic review of the empirical evidence. Landsc. Urban Plan. 97 (3), 147155. https://doi.org/10.1016/j.landurbplan.2010.05.006.

Bröde, P., Fiala, D., Błażejczyk, K., Holmér, I., Jendritzky, G., Kampmann, B., Tinz, B., Havenith, G., 2012. Deriving the operational procedure for the Universal thermal climate index (UTCI). Int. J. Biometeorol. 56 (3), 481494. https://doi.org/10.1007/s00484-011-0454-1.

Bröde, P., Jendritzky, G., Fiala, D., & Havenith, G. (2010). The Universal Thermal Climate Index UTCI in Operational Use.

Cannavo, P., Vidal-Beaudet, L., Grosbellet, C., 2014. Prediction of long-term sustainability of constructed urban soil : impact of high amounts of organic matter on soil physical properties and water transfer. Soil Use Manage 30, 272284. https://doi.org/10.1111/sum.12112.

Chatzidimitriou, A., Chrissomallidou, N., & Yannas, S. (2005). Microclimatic Modifications of an Urban Street in Northern Greece.

Chen, S., Zhang, Z., Chen, Z., Xu, H., Li, J., 2024. Responses of canopy transpiration and conductance to different drought levels in Mongolian pine plantations in a semiarid urban environment of China. Agric. For. Meteorol. 347, 109897. https://doi.org/10.1016/j.agrformet.2024.109897.

Chen, T., Meili, N., Fatichi, S., Hang, J., Tan, P.Y., Yuan, C., 2023. Effects of tree plantings with varying street aspect ratios on the thermal environment using a mechanistic urban canopy model. Build. Environ. 246, 111006. https://doi.org/10.1016/j.buildenv.2023.111006.

Chen, T., Yang, H., Chen, G., Lam, C.K.C., Hang, J., Wang, X., Liu, Y., Ling, H., 2021. Integrated impacts of tree planting and aspect ratios on thermal environment in street canyons by scaled outdoor experiments. Sci. Total Environ. 764, 142920. https://doi.org/10.1016/j.scitotenv.2020.142920.

Dale, A.G., Frank, S.D., 2022. Water availability determines tree growth and physiological response to biotic and abiotic stress in a temperate North American urban forest. Forests 13 (7), 1012. https://doi.org/10.3390/f13071012.

Daudet, F.A., Améglio, T., Cochard, H., Archilla, O., Lacointe, A., 2004. Experimental analysis of the role of water and carbon in tree stem diameter variations. J. Exp. Bot. https://doi.org/10.1093/jxb/eri026.

De Swaef, T., Steppe, K., Lemeur, R., 2009. Determining reference values for stem water potential and maximum daily trunk shrinkage in young apple trees based on plant responses to water deficit. Agric. Water Manage 96 (4), 541550. https://doi.org/10.1016/j.agwat.2008.09.013.

Devakumar, A.S., Prakash, P.G., Sathik, M.B.M., Jacob, J., 1999. Drought alters the canopy architecture and micro-climate of *Hevea brasiliensis* trees. Trees-Struct. Funct. 13, 161–167. https://doi.org/10.1007/PL00009747.

Dietrich, L., Zweifel, R., Kahmen, A., 2018. Daily stem diameter variations can predict the canopy water status of mature temperate trees. Tree Physiol. 38 (7), 941952. https://doi.org/10.1093/treephys/tpy023.

Dimoudi, A., Nikolopoulou, M., 2003. Vegetation in the urban environment : microclimatic analysis and benefits. Energy Build. 8. https://doi.org/10.1016/S0378-7788(02)00081-6.

D'Ippoliti, D., Michelozzi, P., Marino, C., Kirchmayer, U., Analitis, A., Medina-Ramón, M., Paldy, A., Atkinson, R., Kovats, S., Bisanti, L., Schneider, A., Lefranc, A., Iñiguez, C., Perucci, C.A., 2010. The impact of heat waves on mortality in 9 European cities : results from the EuroHEAT project. Environ. Health. https://doi.org/10.1186/1476-069X-9-37.

Drake, J.E., Tjoelker, M.G., Vårhammar, A., 2018. Trees tolerate an extreme heatwave via sustained transpirational cooling and increased leaf thermal tolerance. Glob. Change Biol. 24 (6), 23902402. https://doi.org/10.1111/gcb.14037.

Fiala, D., Havenith, G., Bröde, P., Kampmann, B., Jendritzky, G., 2012. UTCI-Fiala multi-node model of human heat transfer and temperature regulation. Int. J. Biometeorol. 56 (3), 429441. https://doi.org/10.1007/s00484-011-0424-7.

Georgi, N.J., Zafiriadis, K., 2006. The impact of park trees on microclimate in urban areas. Urban Ecosyst. 9 (3), 195209. https://doi.org/10.1007/s11252-006-8590-9.

Gillner, S., Vogt, J., Tharang, A., Dettmann, S., Roloff, A., 2015. Role of street trees in mitigating effects of heat and drought at highly sealed urban sites. Landsc. Urban Plan. 143, 3342. https://doi.org/10.1016/j.landurbplan.2015.06.005.

Girardeau-Montaut, D. (2023). CloudCompare (Version 2.13.alpha) [C++]. www.cloudcompare.org.

Godin, C., 2000. Representing and encoding plant architecture : a review. Ann. For. Sci. 57 (5), 413438. https://doi.org/10.1051/forest:2000132.

Hallé, F., Oldeman, R.A.A., Tomlinson, P.B., Tomlinson, P.B., 1978. Tropical Trees and Forests : An Architectural Analysis. Springer.

Hanna, E., Tait, P., 2015. Limitations to thermoregulation and acclimatization challenge Human adaptation to global warming. Int. J. Environ. Res. Public Health 12 (7), 80348074. https://doi.org/10.3390/ijerph120708034.

Hartmann, C., Moser-Reischl, A., Rahman, M.A., Franceschi, E., von Strachwitz, M., Pauleit, S., Pretzsch, H., Rötzer, T., Paeth, H., 2023. The footprint of heat waves and dry spells in the urban climate of Würzburg, Germany, deduced from a continuous measurement campaign during the anomalously warm years 2018–2020. Meteorol. Z. 4965. https://doi.org/10.1127/metz/2023/1151.

Hendel, M., Colombert, M., Diab, Y., Royon, L., 2014. Improving a pavement-watering method on the basis of pavement surface temperature measurements. Urban Clim. 10, 189200. https://doi.org/10.1016/j.uclim.2014.11.002.

Herpin, S., Mballo, S., Manteau, M., Lemesle, D., Boukouya, A., Dubuc, B., Ledroit, L., Cannavo, P., Demotes-Mainard, S., Bournet, P.E., 2024. A reduced-scale canyon street to study tree climate benefits : summer 2020 data with well-watered apple trees. Sci. Data 11 (1), 1015. https://doi.org/10.1038/s41597-024-03650-0.

Hu, R., Bournez, E., Cheng, S., Jiang, H., Nerry, F., Landes, T., Saudreau, M., Kastendeuch, P., Najjar, G., Colin, J., Yan, G., 2018. Estimating the leaf area of an individual tree in urban areas using terrestrial laser scanner and path length distribution model. ISPRS J. Photogramm. Remote Sens. 144, 357368. https://doi.org/10.1016/j.isprsjprs.2018.07.015.

Huang, Z., Wu, C., Teng, M., Lin, Y., 2020. Impacts of tree canopy cover on microclimate and Human thermal comfort in a shallow Street canyon in Wuhan, China. Atmosphere 11 (6), 588. https://doi.org/10.3390/atmos11060588 (Basel).

IPCC, W. G. 1. (2022). Sixth assessment report of the IPCC, Physical Science Basis Working Group 1's reports.

Jamei, E., Rajagopalan, P., Seyedmahmoudian, M., Jamei, Y., 2016. Review on the impact of urban geometry and pedestrian level greening on outdoor thermal comfort. Renew. Sustain. Energy Rev. 54, 10021017. https://doi.org/10.1016/j.rser.2015.10.104.

Jiao, M., Jenerette, G.D., Zhou, W., Wang, J., Zheng, Z., 2024. Adaptive shading : how microclimates and surface types amplify tree cooling effects? Urban For. Urban Green. 101, 128546. https://doi.org/10.1016/j.ufug.2024.128546.

Khedive, E., Shirvany, A., Assareh, M.H., Sharkey, T.D., 2017. In situ emission of BVOCs by three urban woody species. Urban For. Urban Green. 21, 153157. https://doi.org/10.1016/j.ufug.2016.11.018.

Kjelgren, R., Montague, T., 1998. Urban tree transpiration over turf and asphalt surfaces. Atmos. Environ. 32 (1), 3541. https://doi.org/10.1016/S1352-2310(97)00177-5.

Kleerekoper, L., Van Esch, M., Salcedo, T.B., 2012. How to make a city climate-proof, addressing the urban heat island effect. Resour. Conserv. Recycl. 64, 3038. https://doi.org/10.1016/j.resconrec.2011.06.004.

Konarska, J., Tarvainen, L., Bäcklin, O., Räntfors, M., Uddling, J., 2023. Surface paving more important than species in determining the physiology, growth and cooling effects of urban trees. Landsc. Urban Plan. 240, 104872. https://doi.org/10.1016/j.landurbplan.2023.104872.

Kong, L., Lau, K.K.L., Yuan, C., Chen, Y., Xu, Y., Ren, C., Ng, E., 2017. Regulation of outdoor thermal comfort by trees in Hong Kong. Sustain. Cities Soc. 31, 1225. https://doi.org/10.1016/j.scs.2017.01.018.

Lai, D., Liu, W., Gan, T., Liu, K., Chen, Q., 2019. A review of mitigating strategies to improve the thermal environment and thermal comfort in urban outdoor spaces. Sci. Total Environ. 661, 337353. https://doi.org/10.1016/j.scitotenv.2019.01.062.

Lindberg, F., Grimmond, C.S.B., 2011. Nature of vegetation and building morphology characteristics across a city : influence on shadow patterns and mean radiant temperatures in London. Urban Ecosyst. 14 (4), 617634. https://doi.org/10.1007/s11252-011-0184-5.

Lindén, J., Fonti, P., Esper, J., 2016. Temporal variations in microclimate cooling induced by urban trees in Mainz, Germany. Urban For. Urban Green. 20, 198209. https://doi.org/10.1016/j.ufug.2016.09.001.

Liu, M., Pietzarka, U., Meyer, M., Kniesel, B., Roloff, A., 2022. Annual shoot length of temperate broadleaf species responses to drought. Urban For. Urban Green. 73, 127592. https://doi.org/10.1016/j.ufug.2022.127592.

Lobaccaro, G., Acero, J.A., 2015. Comparative analysis of green actions to improve outdoor thermal comfort inside typical urban street canyons. Urban Clim. 14, 251267. https://doi.org/10.1016/j.uclim.2015.10.002.

Loughner, C.P., Allen, D.J., Zhang, D.L., Pickering, K.E., Dickerson, R.R., Landry, L., 2012. Roles of urban tree canopy and buildings in urban heat island effects : parameterization and preliminary results. J. Appl. Meteorol. Climatol. 51 (10), 17751793. https://doi.org/10.1175/JAMC-D-11-0228.1.

Man, R., Lu, P., Dang, Q.L., 2021. Effects of insufficient chilling on budburst and growth of six temperate forest tree species in Ontario. New For. 52 (2), 303315. https://doi.org/10.1007/s11056-020-09795-1 (Dordr).

Massetti, L., Petralli, M., Napoli, M., Brandani, G., Orlandini, S., Pearlmutter, D., 2019. Effects of deciduous shade trees on surface temperature and pedestrian thermal stress during summer and autumn. Int. J. Biometeorol. 63 (4), 467479. https://doi.org/10.1007/s00484-019-01678-1.

MathWorks, 2013. Alphashape Documentation. MathWorks. https://www.mathworks.com/help/matlab/ref/alphashape.html.

Mballo, S., 2022. Quantification Et Modélisation Des Services Climatiques Rendus Par Les Arbres Dans Une Rue Canyon. Institut Agro Rennes-Angers.

Mballo, S., Herpin, S., Manteau, M., Demotes-Mainard, S., Bournet, P.E., 2021. Impact of well-watered trees on the microclimate inside a canyon street scale model in outdoor environment. Urban. Clim. 37, 100844. https://doi.org/10.1016/j.uclim.2021.100844.

Meili, N., Manoli, G., Burlando, P., Carmeliet, J., Chow, W.T.L., Coutts, A.M., Roth, M., Velasco, E., Vivoni, E.R., Fatichi, S., 2021. Tree effects on urban microclimate : diurnal, seasonal, and climatic temperature differences explained by separating radiation, evapotranspiration, and roughness effects. Urban. For. Urban. Green. 58, 126970. https://doi.org/10.1016/j.ufug.2020.126970.

Météo-France. (2023). https://meteofrance.com/comprendre-climat/france/le-climat-en-france-metropolitaine.

Middel, A., Krayenhoff, E.S., 2019. Micrometeorological determinants of pedestrian thermal exposure during record-breaking heat in Tempe, Arizona : introducing the MaRTy observational platform. Sci. Total Environ. 687, 137151. https://doi.org/10.1016/j.scitotenv.2019.06.085.

Monteith, J.L., Unsworth, M.H., 2013. Principles of Environmental Physics : Plants, Animals, and the Atmosphere - 4th Ed, 4th ed. Elsevier/Academic Press.

Morakinyo, T.E., Kong, L., Lau, K.K.L., Yuan, C., Ng, E., 2017. A study on the impact of shadow-cast and tree species on in-canyon and neighborhood's thermal comfort. Build. Environ. 115, 117. https://doi.org/10.1016/j.buildenv.2017.01.005.

Ngao, J., Cárdenas, M.L., Améglio, T., Colin, J., Saudreau, M., 2021. Implications of urban land management on the cooling properties of urban trees : citizen science and laboratory analysis. Sustainability 13 (24), 13656. https://doi.org/10.3390/su132413656.

Norman, J.M., Welles, J.M., 1983. Radiative transfer in an array of canopies. Agron. J. 75 (3), 481488. https://doi.org/10.2134/agronj1983.00021962007500030016x.

Nowak, D.J., & Dwyer, J.F. (2007). Understanding the benefits and costs of urban forest ecosystems. In Handbook of Urban and Community Forestry in the Northeast (2nd ed., p. 1125).

Oke, T.R., 1973. City size and the urban heat island. Atmos. Environ. 7 (8), 769779. https://doi.org/10.1016/0004-6981(73)90140-6.

Oke, T.R., 1995. The Heat Island of the urban boundary layer : characteristics, causes and effects. In: Cermak, J.E., Davenport, A.G., Plate, E.J., Viegas, D.X. (Eds.), Wind Climate in Cities. Springer, Netherlands, 81107. https://doi.org/10.1007/978-94-017-3686-2_5.

Oliveira, S., Andrade, H., Vaz, T., 2011. The cooling effect of green spaces as a contribution to the mitigation of urban heat : a case study in Lisbon. Build. Environ. 46 (11), 21862194. https://doi.org/10.1016/j.buildenv.2011.04.034.

Park, C.Y., Lee, D.K., Krayenhoff, E.S., Heo, H.K., Hyun, J.H., Oh, K., Park, T.Y., 2019. Variations in pedestrian mean radiant temperature based on the spacing and size of street trees. Sustain. Cities Soc. 48, 101521. https://doi.org/10.1016/j.scs.2019.101521.

Peel, M.C., Finlayson, B.L., McMahon, T.A., 2007. Updated world map of the Köppen-Geiger climate classification. Hydrol. Earth Syst. Sci.

Pimont, F., Dupuy, J.L., Rigolot, E., Prat, V., Piboule, A., 2015. Estimating leaf bulk density distribution in a tree canopy using terrestrial LiDAR and a straightforward calibration procedure. Remote Sens. 7 (6), 79958018. https://doi.org/10.3390/rs70607995 (Basel).

Pisek, J., Ryu, Y., Alikas, K., 2011. Estimating leaf inclination and G-function from leveled digital camera photography in broadleaf canopies. Trees 25 (5), 919924. https://doi.org/10.1007/s00468-011-0566-6.
Pitchers, B., Do, F.C., Pradal, C., Dufour, L., Lauri, P., 2021. Apple tree adaptation to shade in agroforestry : an architectural approach. Am. J. Bot. 108 (5), 732743. https://doi.org/10.1002/ajb2.1652.
Pletsers, A., Caffarra, A., Kelleher, C.T., Donnelly, A., 2015. Chilling temperature and photoperiod influence the timing of bud burst in juvenile Betula pubescens Ehrh. And Populus tremulaL. Trees. Ann. For. Sci. 72 (7), 941953. https://doi.org/10.1007/s13595-015-0491-8.
Qiu, G., Li, H., Zhang, Q., Chen, W., Liang, X., Li, X., 2013. Effects of evapotranspiration on mitigation of urban temperature by vegetation and urban agriculture. J. Integr. Agric. 12 (8), 13071315. https://doi.org/10.1016/S2095-3119(13)60543-2.
Rahman, M.A., Arndt, S., Bravo, F., Cheung, P.K., Van Doorn, N., Franceschi, E., Del Río, M., Livesley, S.J., Moser-Reischl, A., Pattnaik, N., Rötzer, T., Paeth, H., Pauleit, S., Preisler, Y., Pretzsch, H., Tan, P.Y., Cohen, S., Szota, C., Torquato, P.R., 2024. More than a canopy cover metric : influence of canopy quality, water-use strategies and site climate on urban forest cooling potential. Landsc. Urban Plan. 248, 105089. https://doi.org/10.1016/j.landurbplan.2024.105089.
Rahman, M.A., Moser, A., Gold, A., Rötzer, T., Pauleit, S., 2018. Vertical air temperature gradients under the shade of two contrasting urban tree species during different types of summer days. Sci. Total Environ. 633, 100111. https://doi.org/10.1016/j.scitotenv.2018.03.168.
Rahman, M.A., Moser, A., Rötzer, T., Pauleit, S., 2019. Comparing the transpirational and shading effects of two contrasting urban tree species. Urban Ecosyst. 22 (4), 683697. https://doi.org/10.1007/s11252-019-00853-x.
Rahman, M.A., Stratópoulos, L.M.F., Moser-Reischl, A., Zölch, T., Häberle, K.H., Rötzer, T., Pretzsch, H., Pauleit, S., 2020. Traits of trees for cooling urban heat islands : a meta-analysis. Build. Environ. 170, 106606. https://doi.org/10.1016/j.buildenv.2019.106606.
Richards, D., Fung, T., Belcher, R., Edwards, P., 2020. Differential air temperature cooling performance of urban vegetation types in the tropics. Urban For. Urban Green. 50, 126651. https://doi.org/10.1016/j.ufug.2020.126651.
Rizwan, A.M., Dennis, L.Y.C., Liu, C., 2008. A review on the generation, determination and mitigation of Urban Heat Island. J. Environ. Sci. 20 (1), 120128. https://doi.org/10.1016/S1001-0742(08)60019-4.
Ross, J., 1981. The Radiation Regime and Architecture of Plant Stands. Springer, Netherlands. http://link.springer.com/10.1007/978-94-009-8647-3.
Rötzer, T., Moser-Reischl, A., Rahman, M.A., Hartmann, C., Paeth, H., Pauleit, S., Pretzsch, H., 2021. Urban tree growth and ecosystem services under extreme drought. Agric. For. Meteorol. 308309, 108532. https://doi.org/10.1016/j.agrformet.2021.108532.
Santamouris, M., Synnefa, A., Karlessi, T., 2011. Using advanced cool materials in the urban built environment to mitigate heat islands and improve thermal comfort conditions. Sol. Energy 85 (12), 30853102. https://doi.org/10.1016/j.solener.2010.12.023.
Sanusi, R., Johnstone, D., May, P., Livesley, S.J., 2015. Street orientation and side of the Street greatly influence the microclimatic benefits street trees can provide in summer. J. Environ. Qual. 45 (1), 167174. https://doi.org/10.2134/jeq2015.01.0039.
Sanusi, R., Johnstone, D., May, P., Livesley, S.J., 2017. Microclimate benefits that different street tree species provide to sidewalk pedestrians relate to differences in plant area index. Landsc. Urban Plan. 157, 502511. https://doi.org/10.1016/j.landurbplan.2016.08.010.
Sanusi, R., Livesley, S.J., 2020. London plane trees (Platanus x acerifolia) before, during and after a heatwave : losing leaves means less cooling benefit. Urban For. Urban Green. 54, 126746. https://doi.org/10.1016/j.ufug.2020.126746.
Scharwies, J.D., Dinneny, J.R., 2019. Water transport, perception, and response in plants. J. Plant Res. 132 (3), 311324. https://doi.org/10.1007/s10265-019-01089-8.
Sharmin, M., Tjoelker, M.G., Pfautsch, S., Esperon-Rodriguez, M., Rymer, P.D., Power, S. A., 2023. Tree crown traits and planting context contribute to reducing urban heat. Urban For. Urban Green. 83, 127913. https://doi.org/10.1016/j.ufug.2023.127913.
Shashua-Bar, L., & Hoffman, M.E. (2000). Vegetation as a climatic component in the design of an urban street An empirical model for predicting the cooling effect of urban green areas with trees.
Shashua-Bar, L., Pearlmutter, D., Erell, E., 2009. The cooling efficiency of urban landscape strategies in a hot dry climate. Landsc. Urban Plan. 92 (34), 179186. https://doi.org/10.1016/j.landurbplan.2009.04.005.
Shashua-Bar, L., Rahman, M.A., Moser-Reischl, A., Peeters, A., Franceschi, E., Pretzsch, H., Rötzer, T., Pauleit, S., Winters, G., Groner, E., Cohen, S., 2023. Do urban tree hydraulics limit their transpirational cooling? A comparison between temperate and hot arid climates. Urban Clim. 49, 101554. https://doi.org/10.1016/j.uclim.2023.101554.
Sinoquet, H., Stephan, J., Sonohat, G., Lauri, P.É., Monney, Ph, 2007. Simple equations to estimate light interception by isolated trees from canopy structure features : assessment with three-dimensional digitized apple trees. New Phytol. 175 (1), 94106. https://doi.org/10.1111/j.1469-8137.2007.02088.x.
Souch, C.A., Souch, C., 1993. The effect of trees on summertime below canopy urban climates : a case study Bloomington, Indiana. Arboric. Urban For. 19 (5), 303312. https://doi.org/10.48044/jauf.1993.049.
Spangenberg, J., Shinzato, P., Johansson, E., Duarte, D., 2008. Simulation of the influence of vegetation on microclimate and thermal comfort in the city of Sao Paulo. Rev. Soc. Bras. Arborização Urbana 3 (2), 1. https://doi.org/10.5380/revsbau.v3i2.66265.
Steiner, M., Tóth, E.G., Juhász, Á., Diószegi, M.S., & Hrotkó, K. (2014). Stomatal responses of drought and heat stressed (Tilia sp.) leaves. Plants in Urban Areas and Landscape, 710.
Stratópoulos, L.M.F., Duthweiler, S., Häberle, K.H., Pauleit, S., 2018. Effect of native habitat on the cooling ability of six nursery-grown tree species and cultivars for future roadside plantings. Urban For. Urban Green. 30, 3745. https://doi.org/10.1016/j.ufug.2018.01.011.
Su, Y., Liu, L., Liao, J., Wu, J., Ciais, P., Liao, J., He, X., Liu, X., Chen, X., Yuan, W., Zhou, G., Lafortezza, R., 2020. Phenology acts as a primary control of urban vegetation cooling and warming : a synthetic analysis of global site observations. Agric. For. Meteorol. 280, 107765. https://doi.org/10.1016/j.agrformet.2019.107765.
Thierry, J., Herpin, S., Levi, R., Canonne, D., Demotes-Mainard, S., Cannavo, P., Lemesle, D., Brialix, L., Rodriguez, F., Bournet, P.E., 2024. Impact of a water restriction on the summer climatic benefits of trees inside an outdoor street canyon scale model. Build. Environ. https://doi.org/10.1016/j.buildenv.2024.111722.
United Nations, 2019. World Population Prospects Highlights, 2019 Revision Highlights, 2019 revision: Vol. Population Division. Department of Economic and Social Affairs.
Vandendaele, B., Martin-Ducup, O., Fournier, R.A., Pelletier, G., Lejeune, P., 2022. Mobile laser scanning for estimating tree structural attributes in a temperate hardwood forest. Remote Sens. 14 (18), 4522. https://doi.org/10.3390/rs14184522 (Basel).
Wang, Y., Zacharias, J., 2015. Landscape modification for ambient environmental improvement in central business districts – A case from Beijing. Urban For. Urban Green. 14 (1), 818. https://doi.org/10.1016/j.ufug.2014.11.005.
Wong, N.H., Tan, C.L., Kolokotsa, D.D., Takebayashi, H., 2021. Greenery as a mitigation and adaptation strategy to urban heat. Nat. Rev. Earth Environ. 2 (3), 166181. https://doi.org/10.1038/s43017-020-00129-5.
Wujeska-Klause, A., Pfautsch, S., 2020. The best urban trees for daytime cooling leave nights slightly warmer. Forests 11 (9), 945. https://doi.org/10.3390/f11090945.
Yang, C., Yan, F., Zhang, S., 2020. Comparison of land surface and air temperatures for quantifying summer and winter urban heat island in a snow climate city. J. Environ. Manage 265, 110563. https://doi.org/10.1016/j.jenvman.2020.110563.
Yu, K., Van Geel, M., Ceulemans, T., Geerts, W., Ramos, M.M., Sousa, N., Castro, P.M.L., Kastendeuch, P., Najjar, G., Ameglio, T., Ngao, J., Saudreau, M., Honnay, O., Somers, B., 2018. Foliar optical traits indicate that sealed planting conditions negatively affect urban tree health. Ecol. Indic. 95, 895906. https://doi.org/10.1016/j.ecolind.2018.08.047.